



UNIVERSITY OF TWENTE.

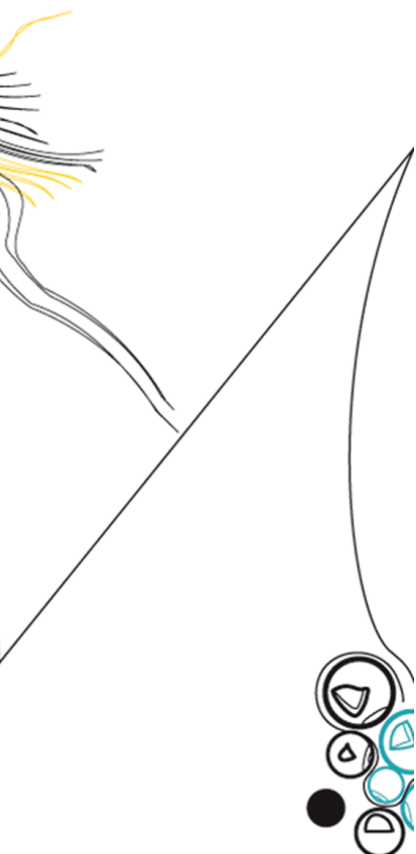
Faculty of Engineering Technology,
Precision Engineering

Controller tuning for disturbance suppression in a piezo damped large stroke flexure hinge

T.P.J. van Hal

M.Sc. Thesis

May 3, 2023



Examination Committee:

prof. dr. ir. D. M. Brouwer

dr. ir. W.B.J. Hakvoort

ir. B. Seinhorst

dr. ir. A.Q.L. Keemink

Precision Engineering
Faculty of Engineering Technology,
University of Twente
P.O. Box 217
7500 AE Enschede
The Netherlands

Summary

The control of conventional servo based mechatronic systems is straightforward. The dynamics of the system can be determined and system parameters can be identified so that a controller can be designed to realize a specified performance. Typically, the performance of the system is mainly determined by the crossover frequency. When considering flexure based mechanisms this presents several difficulties. Usually the design requires a certain compliance in the direction of manipulation but high stiffness in the remaining directions. Since these mechanisms generally contain very little internal damping the higher parasitic eigenfrequencies can become problematic for closed-loop stability. Attempting to circumvent these through design changes can lead to unnecessary complicated mechanisms and can also negatively affect the systems performance. In addition to this, flexure based mechanisms have different mechanical properties with varying degrees of deflection and therefore have changing frequency responses. This increases the difficulty to reach performance goals at all angles of deflection. One way to overcome these problems is through the use of piezoelectric elements to apply damping in the system and to reach performance objectives through all angles of deflection.

Recently, a large stroke flexure hinge has been developed at the University of Twente to demonstrate the use of piezoelectric elements and their ability to identify the effects of the higher order parasitic eigenfrequencies. This research focuses on the next step in the process; controlling the piezoelectric elements in such a way that these negative parasitic effects are successfully damped. Typically, some form of Resonance control is used, as other methods will lead to excessive spillover. For this control problem a single parasitic eigenmode of the flexure hinge is chosen.

In this work, two different control methods are investigated, Positive Position Feedback (PPF) and Resonant Feedback Control (RFC). These controllers are optimally tuned to provide the greatest performance. Through simulations it is found that both controllers show comparable results. These results are tested experimentally and here it is found that the same optimally tuned PPF controller was successful in reducing the parasitic resonance for several deflections of the mechanism. RFC was unsuccessful as it led to an unstable system.

Contents

1	Journal Paper	1
1.1	Controller tuning for disturbance suppression in a piezo damped large stroke flexure hinge	1
2	References	11
	Appendices	13
A	Shaker element design	13
A.1	Requirements	13
A.2	Constraints	13
A.3	Dimensions	14
B	Simulation results	15
B.1	System Model Frequency Response	15
B.2	Parameter Sweeps	15
C	Experimental setup	23
D	Experimental results	24
D.1	Frequency Response Estimate	24
D.2	Optimally tuned PPF controller	24
D.3	Frequency variation	27
D.4	Gain/damping variation	27

Controller tuning for disturbance suppression in a piezo damped large stroke flexure hinge

Precision Engineering
Faculty of Engineering Technology
2023(1):1–11
©The Author(s) 2023
www.utwente.nl/

UNIVERSITY OF TWENTE.

T.P.J. van Hal¹

Abstract

Many concurrent precision mechanisms have flexure joints. These mechanisms are predictable since flexure joints avoid backlash and friction. However, there are drawbacks in the form of parasitic eigenmodes that can adversely affect performance. This is especially true when such structures are controlled in a deflected state. One way to counter this is through the implementation of Active Vibration Damping by placing piezo elements at key points in the structure. These piezo elements can be controlled in such a way that they suppress parasitic vibrations. The control systems investigated in this work are Positive Position Feedback (PPF) and Resonant Feedback Control (RFC). The effect of the parameters of these controllers on their ability to achieve damping of parasitic resonances is studied and a tuning method is designed. This method consists of selecting a performance criterion and performing a grid search that leads to optimal controller parameters. The performance criterion was the H2 norm of the transfer from force to displacement. The resulting PPF controller showed an average simulated improvement of the H2 norm of 23.4% with respect to the uncontrolled case. RFC showed an average simulated improvement of the H2 norm of 24.2% with respect to the uncontrolled case. These results have been tested experimentally and PPF was shown to be successful in reducing the parasitic resonance frequency for all states of deflection. Resonance peak height has been reduced by an average of 13 dB. During testing RFC resulted in instability and was unsuccessful in reducing resonance peak height.

Keywords

Flexures, Active Vibration Damping, Positive Position Feedback, Resonant Feedback Control

Introduction

As the field of Precision Engineering developed, the demand for smaller mechanisms rose. It is difficult to reach these increasing performance goals with the use of typical bearing based mechanisms as these show hysteresis and friction effects from which the repeatability suffers greatly.

Flexures are often used to combat these effects as they inherently lack any form of play. Mechanisms constructed of these flexures are therefore highly predictable and this makes for excellent repeatability [1]. Nevertheless, flexure mechanisms have drawbacks of their own and can make designing them difficult.

Flexure mechanisms are designed on the premise that they allow for a degree of freedom (DOF) in a certain direction while also providing a degree of constraint (DOC) in the remaining directions. However, flexures are only finitely stiff in the constrained directions, providing finite DOC's. This is even more so when the mechanism is deflected as this greatly reduces the support stiffness of the flexures [2]. Counteracting these negative effects can be done through essentially two methods; to either improve the mechanisms design and therefore better the DOC's or to somehow apply damping into the structure and thereby reducing the negative effects of the decreasing DOC's.

Altering designs to overcome the decrease in DOC generally leads to an increase in mechanism complexity and possibly a reduction in nominal performance. Additionally, if the maximum support stiffness is already reached an improvement in design to overcome the decrease in

DOC is no longer possible [3]. Therefore, it is of more interest to investigate the application of damping into an existing flexure mechanism. Recent studies have shown that piezoelectric elements placed at key points in the mechanism can act as active material [4]. These elements are used in pairs of sensors and actuators to couple voltage to deformation and thereby are able to detect and control unwanted effects of the DOC's [5].

There has been some research into the exact placement of these piezo-patches for the case of large stroke mechanisms. The approach was to take into account that there are strain limitations on the piezo elements and these need to be placed in locations of high modal strain but limited nominal strain. For a cross hinge case in [2] this proved to be at the base of the flexures where they are attached to the rigid world. Simulations have shown that active material can be a feasible vibration suppression method in large deformation flexures [6].

Extensive research has been performed regarding the control of these piezoelectric elements which has yielded several feasible controllers; Positive Position Feedback [7; 8], Direct Velocity feedback [9; 10], Negative Derivative Feedback [8], Resonant Feedback Control [7], and Integral Resonant Control [11; 12].

¹Precision Engineering, Faculty of Engineering Technology, University of Twente, Enschede, The Netherlands

Corresponding author:

Theo van Hal: s1018140

Email: t.p.j.vanhal@student.utwente.nl

Naturally, the choice of the control algorithm affects the ability to successfully apply damping on a flexure mechanism and reducing known parasitic resonance frequencies. This choice is generally left to the designer, as each of these control algorithms have advantages and drawbacks. However, the aforementioned control schemes for Active Vibration Damping can all be considered resonant control techniques. For flexure mechanisms generally only a select number of vibration modes are relevant and as such in these control techniques a first- or second order compensator is used to control the relevant modes [8].

Aside from the algorithm, the controller settings generally require manual tuning to achieve satisfactory performance [13]. Additionally, little is known regarding these controllers for a large deformation case as most of them have been studied for small stroke mechanisms.

To assess how a large deformation case affects the piezo patches' ability to register parasitic resonances and apply damping accordingly, this work will focus on a large stroke flexure hinge case. A demonstrator has been developed at the University of Twente [14]. The aim of this research is to analyze an adaptation of this demonstrator by selecting a single parasitic mode for which a suitable controller will be selected. For the controller, a tuning method is proposed to avoid relying on manual tuning. This method consists of selecting an optimisation criterion, applying design constraints, and choosing a search algorithm. This method leads to the selection of optimally tuned control parameters which will be tested experimentally.

In the remainder of this paper, the large stroke flexure hinge is introduced and a control scheme for Active Vibration Damping is presented. Then, the tuning method is proposed and the optimally tuned controllers are tested experimentally. Finally, these results are discussed and conclusions are drawn.

Large Stroke Flexure Hinge case

Previous research has led to the design of a flexure hinge to demonstrate a novel approach of damping performance limiting modes in large stroke flexures [14]. The hinge consists of four leaf flexures, which are connected to a long shuttle by effectively stacking two cross hinges on top of each other. The orientation and dimensions of the flexures have been selected such that minimal pivot shift is present under deflection [15]. On the end of the stage a brass mass of 1 kg is fixed. On the leaf flexures, stacks of piezoelectric elements are placed to use as sensor-actuator pairs. On the shuttle an actuator and encoder are mounted to provide accurate rotation.

It was shown that the demonstrator is able to accurately register several of the analysed modes present in the nominal movement plane. This is the case when the stacks of piezoelectric elements are placed at the base of the flexures, i.e. where the flexures are connected to the fixed world. These locations are known to be subject to high modal strain but relatively low nominal strain [2; 6].

The demonstrator was previously used to sense parasitic modes and analyse their effect on the nominal movement transfer from torque M to angle of deflection θ . It was found that not all of the studied modes had a clear effect,

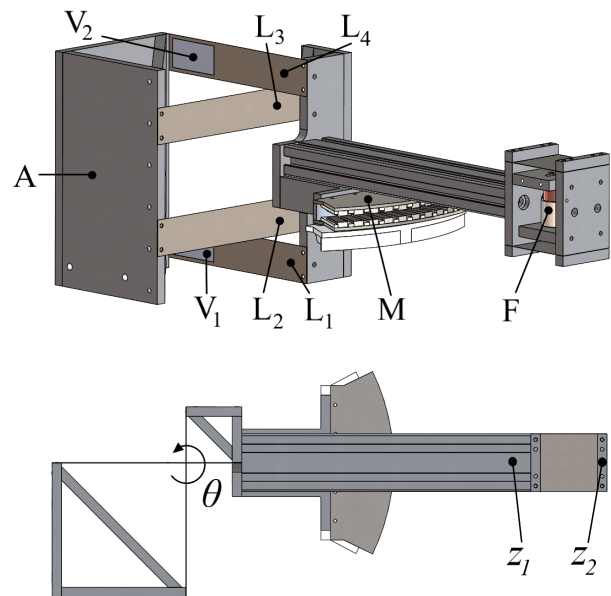


Figure 1. Simplified rendering of system model in undeflected state, with leafsprings (L), piezos (V), fixed base (A), torque (M), force (F), angle (θ), and position (z)

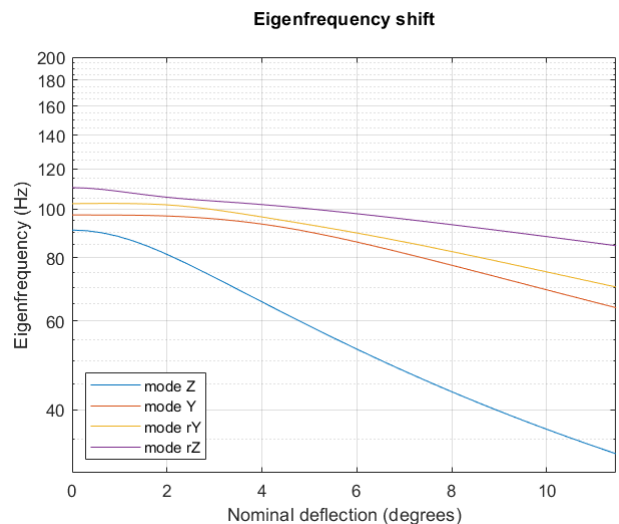


Figure 2. Eigenfrequency shift over nominal deflection (θ) in accordance to naming convention in [14]

mode Z was unobservable through the nominal transfer. However, these out-of-plane modes can have a detrimental effect on overall performance. Therefore, for the remainder of this work only these out-of-plane modes are considered as parasitic movement and the effect of the remaining modes will be disregarded. To study the effects of the parasitic resonances on this out of plane movement, the demonstrator is supplemented with a shaker element. Details on the design of this shaker are included in appendix A. This is a driven two-leaf straight guide. Additionally, some changes have been made to the frame to reduce its compliance. A representation of the modified system is shown in figure 1.

The system is analysed through the use of modified SPACAR software to identify the parasitic modes and their corresponding eigenfrequencies and how these develop under deflection [2; 6]. The simulated results for the first

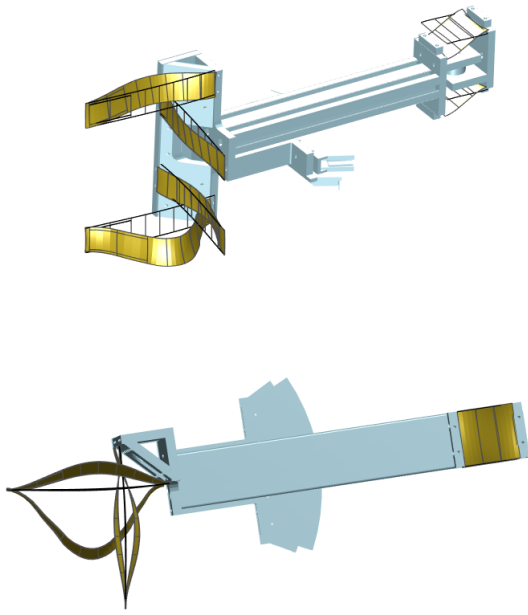


Figure 3. Identified mode shape of interest at 8.5 degrees of deflection. Base structure omitted for improved clarity

four parasitic resonance frequencies are shown in figure 2. The naming convention used in this figure is in accordance to that in previous research [14]. From this it becomes clear that the first parasitic resonance frequency decreases most under deflection of the nominal stage. The corresponding parasitic mode shape is shown in figure 3 and can be best described as a translation in z-direction of the end-effector. This mode is selected as the mode of interest for which to apply active vibration damping. Modal damping of 0.5% is assumed to represent natural internal damping. Figure 4 shows the simulated frequency response from force F to displacement z_1 at 8.5 degrees nominal deflection. Here, the peaks at 0.8 Hz and 8 Hz correspond with the designed compliance of the nominal movement of the hinge and the shaker element, respectively. After those, the most prominent resonance is at 41 Hz and this corresponds with the mode shape shown in figure 3. The remaining simulated frequency responses of the system can be found in appendix B.

Figure 3 shows that for the mode of interest leafsprings 1 and 4 experience great strain whereas leafsprings 2 and 3 appear to experience relatively little strain. Furthermore, as the strain in leafsprings 2 and 3 is mostly torsional their contribution is hereafter disregarded. Leafspring 1 and 4 will be referred to as leafspring A and B, respectively, for the remainder of this work.

Control problem and objective

To achieve the required damping of the parasitic resonance frequency the system is represented in the generalised plant setting, which is shown in figure 5. Here, the transfer from torque M to deflection angle θ represents the main loop (nominal motion of the hinge) and the transfer from force F to displacement z_1 represents the performance loop (parasitic motion of the hinge). The transfer from force F to z_2 represents the movement of the shaker mass and will be

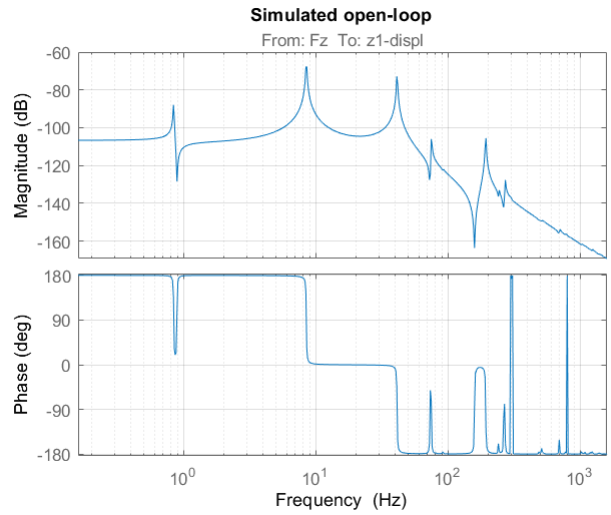


Figure 4. Simulated bode diagram from force F_z to displacement z_1 at 8.5 degrees nominal deflection. Additional figures in appendix B

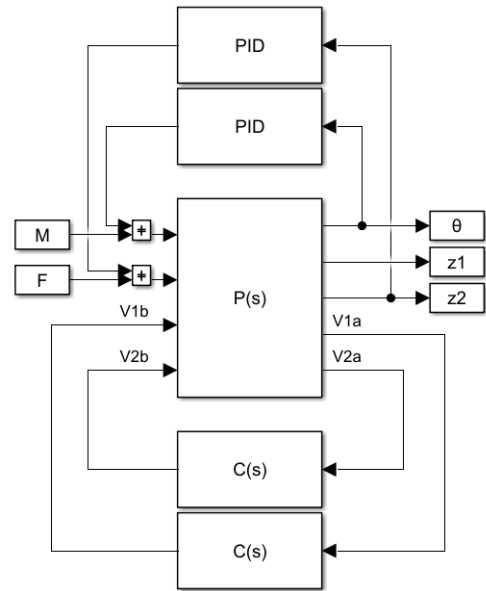


Figure 5. Schematic for proposed active vibration control

disregarded for the remainder of this work. Both sets of piezoelectric elements are controlled through a controller, $C(s)$, in order to improve the performance of the transfer from force F to displacement z_1 . For this case, both sets of piezoelectric elements are controlled by independent identical controllers to reduce complexity.

For Active Vibration Damping there is a multitude of available controller varieties. However, in this work only two controllers will be considered. These are Positive Position Feedback (PPF) and Resonant Feedback Control (RFC). PPF has first been introduced by [16] and has since been studied extensively. One of the main advantages of PPF is that it is easily implemented and therefore has been applied to many flexible systems for Active Vibration Damping [17]. RFC is similar to PPF as it is also easily implemented. However,

as RFC mirrors PPF, it has almost opposite characteristics which makes for an interesting comparison.

Positive Position Feedback

PPF is a second order controller. Its transfer is given by [8].

$$C(s) = \frac{K\omega_c^2}{s^2 + 2\zeta_c\omega_c s + \omega_c^2} \quad (1)$$

Where K is the controller gain, ζ_c is the controller damping, and ω_c is the controller frequency. Figure 6 shows a typical bode plot for a PPF controller. This shows that, besides the intentional resonance behaviour, PPF has low pass filter characteristics. At ω_c this controller provides -90° of phase with respect to the input. Since this is positively fed back it can be considered negative velocity feedback and therefore provides a damping force at the controller resonant frequency [8].

PPF is considered to be insensitive to spillover due to its high frequency roll off. However, it is very sensitive to low frequency disturbances which causes a worsening performance of the closed loop system at low frequencies [7].

Resonant Feedback Control

RFC is also a second order controller and its transfer is given by [7].

$$C(s) = \frac{Ks^2}{s^2 + 2\zeta_c\omega_c s + \omega_c^2} \quad (2)$$

Where K is the controller gain, ζ_c is the controller damping, and ω_c is the controller frequency. Figure 6 shows a typical bode plot for a RFC controller. This shows that, besides the intentional resonance behaviour, RFC has high-pass filter characteristics. At ω_c this controller provides 90° of phase with respect to its input. However, as this is positive phase, for RFC to provide cancellation it is fed back negatively.

RFC is insensitive to low frequency disturbances. However, while closed-loop stability can be guaranteed when the sensor/actuator pair is perfect, uncertainty at high frequencies such as out of bandwidth dynamics may destabilize the closed-loop system [7].

Resonant control vs Pure Damper

Both PPF and RFC are of the resonant controller type. In figure 6 the typical bode diagram of a pure damper is included in addition to those of both resonant controllers. From this can be seen that a pure damper provides 90° of phase at all frequencies while resonant controllers only provide 90° of phase at their respective resonant frequencies. Consequently, a pure damper has significantly more spillover in comparison and therefore, resonant controllers are highly favorable in Active Vibration Damping.

Active Damping Performance

As previously indicated, the aim is to apply damping on the resonance frequency in the transfer from force F to displacement z_1 for the end-effector. This is achieved by controlling piezoelectric elements that are placed on the leaf

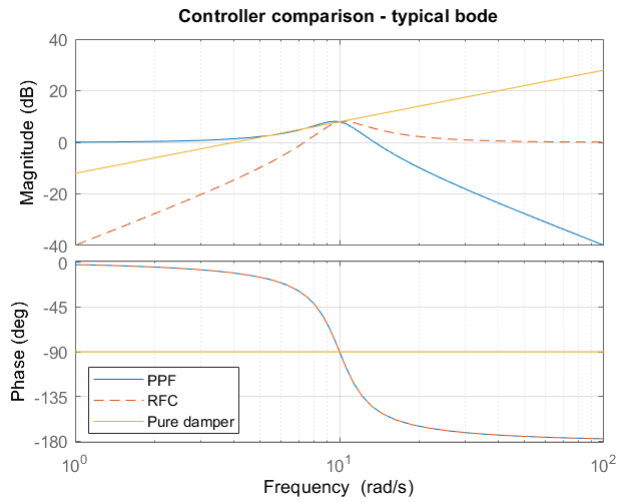


Figure 6. Typical bode diagram of PPF and RFC controllers (both with $K = 1$, $\zeta_c = 0.2$, $\omega_c = 10$), along with that of a pure damper

flexures. However, in order to assess the performance of the applied active damping control, a performance criterion is needed. The transfer from force F to displacement z_1 was selected as the performance loop as this represents the parasitic motion of the intermediate mass. To calculate the performance gain the H2 norm of the transfer from force F to displacement z_1 is chosen. The H2 norm is defined as [18]:

$$\|H\|_2 = \sqrt{\frac{1}{2\pi} \int_{-\infty}^{\infty} \text{Trace}[H(j\omega)^H H(j\omega)] d\omega} \quad (3)$$

As can be seen from equations 1 and 2, for both PPF and RFC three control parameters are to be determined. For the selection of these parameters, previous research often relied on manual tuning by the designer. In this work however, manual tuning is avoided by using a tuning method. In this, the relations between the control parameters and the resulting change in H2 norm of the performance loop are determined through a grid search. Of these, the parameters that result in the lowest H2 norm will be selected as optimal control parameters. The resulting optimal controllers will be tested experimentally.

Optimal parameter tuning

For both PPF and RFC the parameter sweeps are performed within the same parameter windows. In order to increase the applicability of the results, the parameters have been normalized with respect to the plant properties, i.e. the controller gain factor is expressed as a ratio of the gain margin of the voltage to voltage transfer of leafspring A and the controller frequency is expressed as a ratio of the parasitic resonance frequency.

This results in the following parameter windows:

$$0.3 \leq \bar{K} \leq 1 \quad (4)$$

$$0.01 \leq \bar{\zeta} \leq 0.5 \quad (5)$$

$$1 \leq \bar{\omega} \leq 3 \quad (6)$$

Where:

$$\bar{K} = \frac{K_c}{gm} \quad (7)$$

$$\bar{\zeta} = \zeta_c \quad (8)$$

$$\bar{\omega} = \frac{\omega_c}{\omega_{par}} \quad (9)$$

When \bar{K} approaches 1, the system has little to no stability margin. To achieve a system design with robust stability the chosen stability margin is the minimum distance of the representation of the open-loop transfer to the point -1,0 on the Nyquist diagram. This minimum distance is equal to the inverse of the maximum of sensitivity, M_S^{-1} [19]. The maximum of sensitivity is calculated using the L_∞ norm which is defined as [18]:

$$M_S = \|S\|_{L_\infty} = \max_{\omega \in R} |S(j\omega)| \quad (10)$$

The minimum for the minimum distance is set at 0.3, i.e. $M_S^{-1} \geq 0.3$, controller parameter combinations that result in less stability margin are disregarded.

As was shown in figure 2 the angle of deflection is of great influence on the eigenfrequency of the parasitic mode. The amount of deflection is presumed to also affect the performance of the control parameter combinations as well as their sensitivity margin. Therefore these simulations are performed for four states of the system, equidistantly spaced between minimum and maximum deflection. This results in the following states; undeflected, 2.8 degrees nominal deflection, 5.7 degrees nominal deflection, and 8.5 degrees nominal deflection.

Sensitivity surface

The simulated results can be represented in 4D for each controller for each state of deflection. Figure 7 shows the results for when PPF is enabled at 8.5 degrees nominal deflection. Figure 8 shows the results for when RFC is enabled at 8.5 degrees nominal deflection. Here, the x, y, and z coordinates correspond to the normalized controller parameters and the magenta contour lines correspond to the sensitivity margin. The points that lie within this sensitivity margin surface represent feasible controllers with the coordinates set as their parameters. The colour scale indicates the resulting H2 norm of the transfer from force F to displacement z_1 of the end-effector for when the respective controller is enabled. Figures for the remaining states of deflection are included in appendix B.

For both PPF and RFC an absolute minimum can be found within the parameter windows. However, dealing with potential uncertainty, an optimal region is defined for each of the sensitivity surfaces. In this region the H2 norm value of the performance loop differs less than two percent from the absolute minimum, i.e. $H_{2,opt} \leq 1.02 \cdot H_{2,min}$. These regions are included in figures 7 and 8 in red.

From these simulated results it becomes clear that for both PPF and RFC the stability margin of 0.3, represented by the magenta lines, is mainly determined by the controller

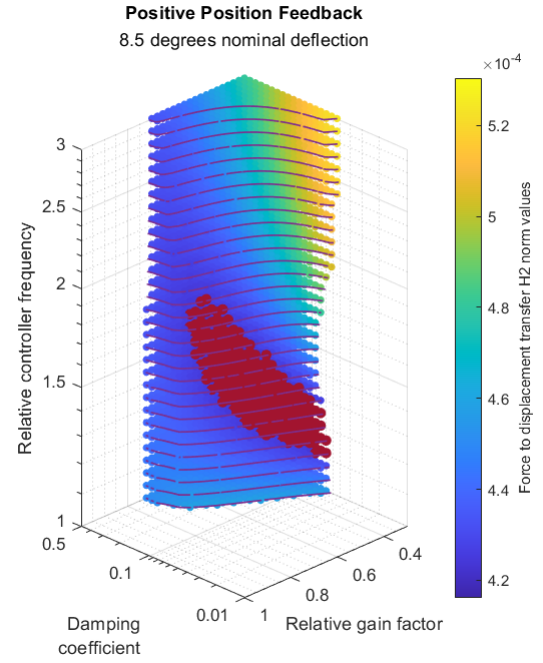


Figure 7. Sensitivity surface and corresponding H2 norm values for PPF control under 8.5 degrees of deflection with in red the optimal region (< 2%). Additional figures in appendix B

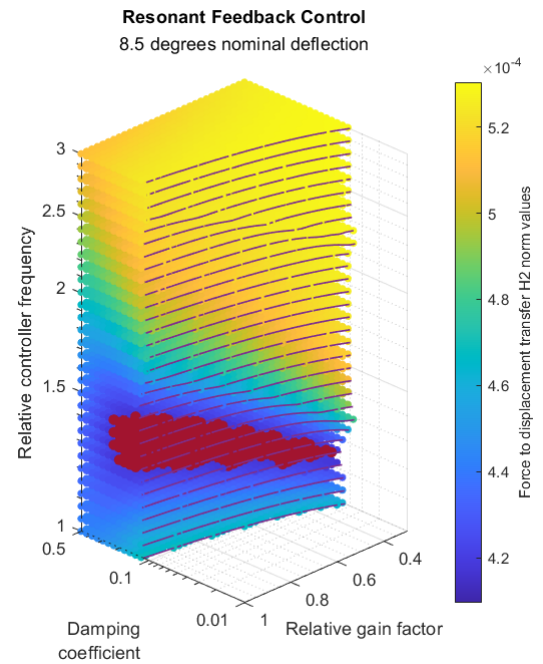


Figure 8. Sensitivity surface and corresponding H2 norm values for RFC control under 8.5 degrees of deflection with in red the optimal region (< 2%). Additional figures in appendix B

gain and controller damping factors, while the controller frequency has much less effect, as the contour of these lines largely retains its shape with increased controller frequency.

The optimal region for PPF shows a strong correlation between controller frequency on one side and the combination of gain and damping on the other side. This is such that for an increase in controller frequency both the controller gain and controller damping should be increased as well in order to achieve similar results. Nevertheless,

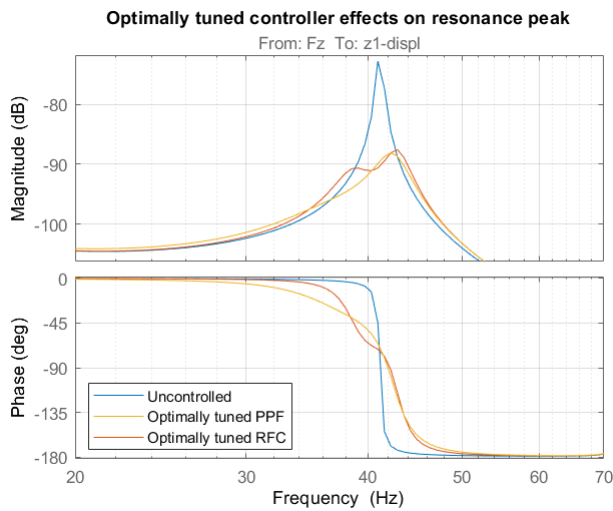


Figure 9. Simulated frequency response from force F to displacement z_1 under 8.5 degrees nominal deflection without damping, with PPF damping, and with RFC damping

outside of this minimal region, PPF shows relatively good performance as well as a strong ability to overcome model uncertainties indicating good performance robustness.

The optimal region for RFC is bound by a narrow window of controller damping factor, a narrow window of controller frequency, and a wide window of controller gain factor. Therefore the performance of the enabled RFC controller is mostly dictated by its damping and frequency. As the damping factor is dimensionless and the controller frequency is set relative to the parasitic eigenfrequency this implicates that the performance of the RFC controllers is mostly determined by the accuracy of the system model. As the performance outside of the minimal region lessens more quickly compared to that of PPF it stands to reason that RFC controllers are therefore less able to overcome model uncertainties.

Angle of deflection

Comparing the sensitivity surface results for the 8.5 degrees nominal deflection state with those for the remaining deflected states, found in appendix B, it appears that, although the absolute values for the H2 norm differ greatly, the shape of the sensitivity surfaces differs little under deflection. This implies that the closed-loop stability of the system with active damping enabled is largely unaffected by the angle of deflection. Furthermore, the optimal tuning regions are located in approximately the same locations for all deflected states. This implies that a single set of normalized parameters can achieve near-optimal performance for all angles of deflection. This is the case for both PPF and RFC controllers. However, it should be noted that these parameters are in normalized form, relative to the plant properties. As previously shown, the plant properties are affected by the angle of deflection and the controllers will still have to account for this.

For each of the studied deflected states, the parameter sets resulting in the absolute minimum H2 norm are determined. The means of these parameters have been selected as the optimally tuned control parameters. This is done for both

Table 1. Optimally tuned control parameters

	\bar{K}	$\bar{\zeta}$	$\bar{\omega}$
PPF	0.51	0.12	1.30
RFC	0.67	0.09	1.25

Table 2. Simulated effects of optimally tuned controllers on parasitic resonances in the frequency response from force F to displacement z_1

	θ	ω_{par}	Open-loop Magnitude	H2 norm Reduction	Freq. Peak Reduction
PPF	2.8 °	74 Hz	-88.5 dB	24.1%	16.5 dB
	5.7 °	54 Hz	-78.2 dB	25.1%	16.0 dB
	8.5 °	41 Hz	-72.8 dB	21.0%	15.3 dB
RFC	2.8 °	74 Hz	-88.5 dB	24.2%	15.5 dB
	5.7 °	54 Hz	-78.2 dB	26.1%	15.5 dB
	8.5 °	41 Hz	-72.8 dB	22.4%	14.8 dB

PPF and RFC. The resulting normalized parameters are listed in table 1.

For each of the deflected states, the parasitic frequency and the resonance peak height are determined. These are listed in table 2. For the determination of the resonance peak height a modal damping of 0.5% is assumed. Additionally, table 2 lists the effects of the optimally tuned controllers on the H2 norm of the transfer from force F to displacement z_1 and on the resonance peak height of the transfer from force F to displacement z_1 . From this it can be concluded that, for both PPF and RFC, the optimally tuned controllers are successful in reducing the parasitic resonance peaks for all simulated states of deflection. However, it also shows that, although RFC performs slightly better in reducing the H2 norm, the frequency peak is reduced less when compared to PPF. This effect is illustrated in figure 9. It shows the simulated transfer from force F to displacement z_1 under 8.5 degrees nominal deflection, for the open-loop system, the system with optimally tuned PPF, and the system with optimally tuned RFC. The magnitude diagram is zoomed in around the resonance frequency at 41 Hz. Here, it can be seen that, while the resonance peak is lower for the optimally tuned PPF controller, at low frequencies the magnitude is slightly higher. As the H2 norm is defined by equation 3 this results in a slightly higher H2 norm for PPF compared to RFC.

Experimental Validation

To assess whether the model is an accurate representation of the system, the simulated results are tested experimentally. The major components of the experimental setup are listed in table 3 and a schematic representation of the experimental setup is shown in figure 10. Pictures of the experimental setup are included in appendix C.

Both the nominal motion stage and the shaker element are actuated through a PID controller. The methods through which these controllers are designed are given by [28]. Their cross-over frequencies are 5 Hz and 15 Hz, respectively. Since both controllers are needed purely for retaining a given

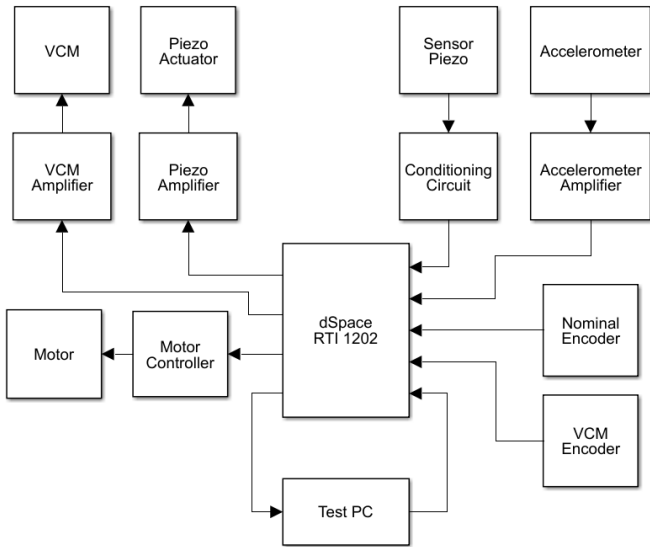


Figure 10. Schematic representation of the experimental setup

position of their respective stage and therefore have no effect on the performance of the active damping their exact design will not be discussed further.

Multiple tests are performed in order to asses whether the optimally tuned PPF and RFC controllers are successful in damping the chosen parasitic resonance frequency peak. First, the system was identified without Active Vibration Damping to determine its ability to correctly register the parasitic resonance for the deflections in accordance to those of the simulations; undeflected, 2.8 degrees deflected, 5.7 degrees deflected, and 8.5 degrees deflected.

The dynamics of the system are then identified with Active Vibration Damping enabled for the four states of deflection. This is tested for both optimally tuned controllers with parameters as listed in table 1. In addition to the designed controllers, four sub-optimal controllers will be tested. The controller parameters of these are chosen such that they are pairwise located on opposite sides of the optimally tuned controllers alongside the two axes of the sensitivity surface and outside of the minimal region. These variations are listed in table 4 for both PPF and RFC. As the parameters in both table 1 and 4 are in normalized form, the previous system

Table 3. Major components of experimental setup

	Component	Description
<i>Nominal Stage</i>	Motor	Tecnotion UM3 [20]
	Motor controller	Escon 50/5 [21]
	Encoder	RLS LM10 [22]
	Accelerometer	Endevco 7703A-1000 [23]
	Sensor	M5628-P1 [24]
	Actuator	M5628-P1 [24]
	Flexures	RVS 14.310 [25] 139 x 35 x 0.3 mm
<i>Shaker Stage</i>	Motor	Akribis AVM 30-15 [26]
	Encoder	RLS LM13 [27]
	Flexures	RVS 14.310 [25] 79 x 60 x 0.2 mm

Table 4. Parameter variations for applied controllers

Combination	\bar{K}	$\bar{\zeta}$	$\bar{\omega}$
<i>PPF 1</i>	0.51	0.12	1.58
	0.51	0.12	1.05
	0.35	0.09	1.30
	0.65	0.23	1.30
<i>RFC 1</i>	0.67	0.09	1.39
	0.67	0.09	1.15
	0.44	0.07	1.25
	0.88	0.12	1.25

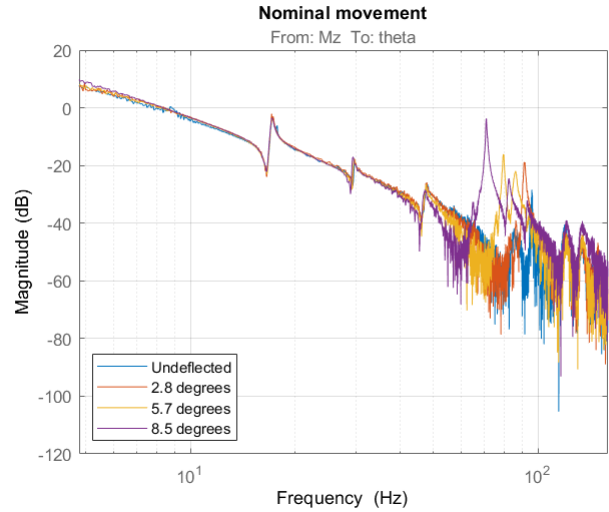


Figure 11. Frequency response from torque M to angle of deflection θ for multiple deflections

measurements were used to determine absolute controller parameters.

The dynamics of the system are identified through the use of a chirp signal with an amplitude of 100 mA from 10 to 200 Hz as the simulated results have shown this to be the main region of interest.

Results

The results of the system identification are shown in figures 11, 12, and 13. More details on how these results are obtained are given in appendix D.

Figure 11 shows the measured frequency response from torque M to angle of deflection θ for the four states of deflection; undeflected, 2.8 degrees nominal deflection, 5.7 degrees nominal deflection, and 8.5 degrees nominal deflection. Figure 12 shows the measured frequency response data from force F to displacement z_1 and figure 13 shows the measured frequency response from voltage $V1a$ to voltage $V1b$ for leafspring A. The full 5x4 system frequency response data - with inputs $M, F, V1a, V2a$ and outputs $\theta, z_1, z_2, V1b, V2b$ - is included in appendix D. As was expected from the simulation results, both the frequency responses from figures 12 and 13 show a resonance peak that shifts from 56.4 Hz for the undeflected state to 30.1 Hz for 8.5 degrees nominal deflection. As the resonance peaks from force F to displacement z_1 correspond to those from voltage $V1a$ to voltage $V1b$, the piezoelectric elements couple with

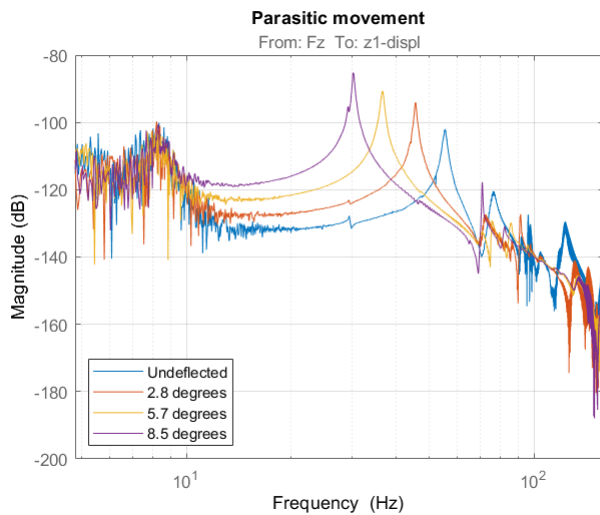


Figure 12. Frequency response from force F to displacement z_1 for multiple deflections

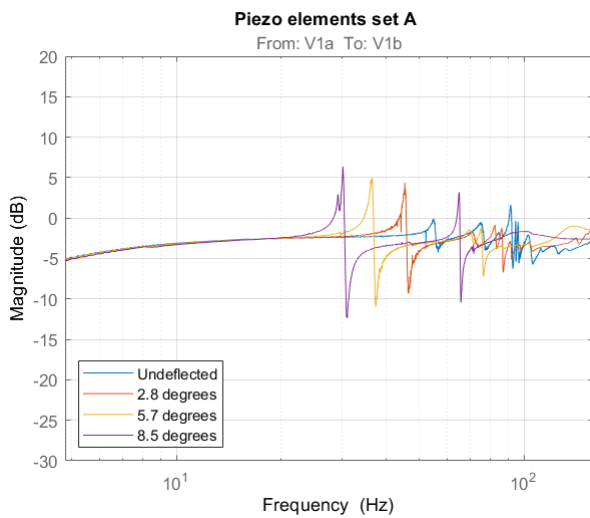


Figure 13. Frequency response from voltage $V1a$ to voltage $V1b$ for leafspring A for multiple deflections

the displacement effect. There is no noticeable effect of these resonances in the frequency response from torque M to angle of deflection θ which shows that the mode from figure 3 is unobservable in the nominal movement.

Additionally, figure 12 shows a resonance peak at 8 Hz for all states of deflection. This corresponds to the nominal compliance of the shaker element, as it is independent of the angle of deflection. This is in accordance to the simulated frequency response.

Figure 11 shows several unexpected collocated resonance peaks, which are at 17 Hz, 29 Hz, and 46 Hz. These are not present in the simulated frequency response. However, as these appear to be independent of the angle of deflection they are assumed to be caused by unknown dynamics outside of the bounds of the system model and are therefore disregarded.

The controller parameters were tuned such that the controllers were assumed to provide near-optimal performance for multiple deflected states of the nominal motion stage. However, as these parameters are in normalized form, for

each of the deflected states both the gain margin and the parasitic eigenfrequency are needed. These can be gathered from the results of the system identification. Figure 13 indicates that the gain margin of leafspring A varies very little with respect to a change in angle of deflection. From this it can be concluded that, out of the three controller parameters, only the absolute controller frequency varies greatly.

PPF

Figure 14 shows the resulting frequency responses from force to displacement with PPF control enabled, as depicted in figure 5, for multiple displacements. The amount of achieved damping for these displacements is listed in table 5. From these it can be seen that the optimally tuned PPF controller can successfully dampen the parasitic resonance across multiple deflections. Additionally, the achieved resonance peak reductions are similar to those reached in simulated results.

The achieved damping effect is less for the undeflected state compared to those for deflected states, however this was to be expected. As figure 2 showed, the eigenfrequency for the parasitic mode of figure 3 drops drastically under deflection. In the undeflected state the eigenfrequency is close to the eigenfrequencies of several other modes that were previously disregarded. This implicates a greater contribution of those modes on the frequency response from force F to displacement z_1 than previously assumed.

The remaining frequency response diagrams of the system with the optimally tuned PPF controller enabled are included in appendix D.

Table 5. Experimental effects of optimally tuned PPF controller on parasitic resonances for multiple deflections

<i>Nominal Deflection</i>	ω_{par}	<i>Open-loop Magnitude</i>	<i>Freq. Peak Reduction</i>
Undeflected	56.4 Hz	-102 dB	6 dB
2.8 degrees	45.6 Hz	-94.1 dB	13.9 dB
5.7 degrees	36.7 Hz	-90.7 dB	15.3 dB
8.5 degrees	30.1 Hz	-85.2 dB	16.8 dB

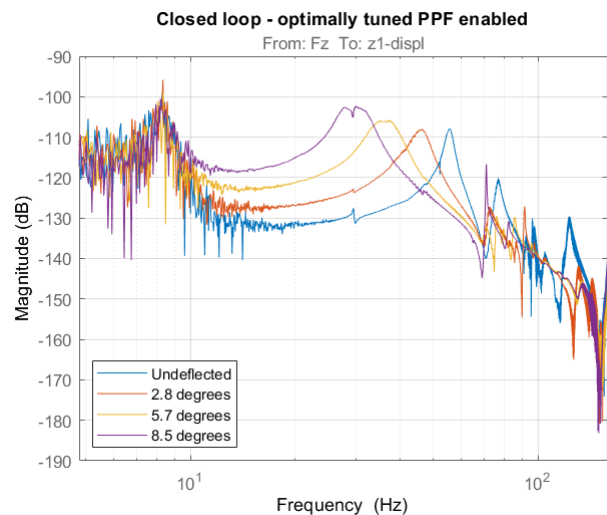


Figure 14. Frequency response from force F to displacement z_1 for multiple deflections with optimally tuned PPF enabled

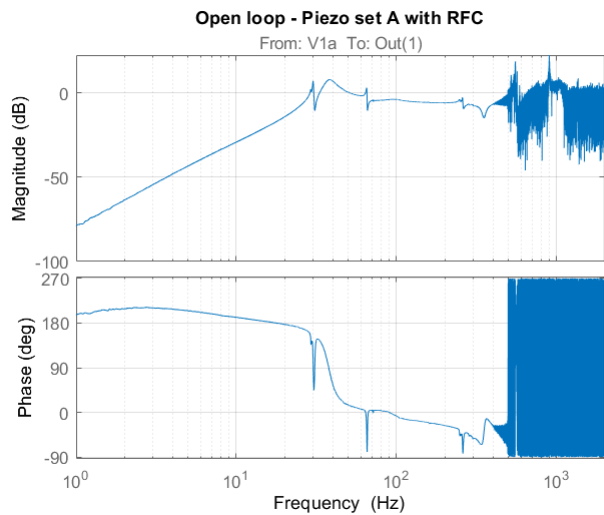


Figure 15. Open loop bode plot for leafspring A with the optimally tuned RFC controller

RFC

When RFC is enabled similarly to PPF in the previous section simulation results indicated an increase in performance was to be expected. However, with the values for g_m and ω_{par} determined and the controller parameters set to those listed in table 1, enabling the controllers led to immediate instability. This is in spite of the selected stability margin when the parameters were determined. Only after significantly lowering the controller parameters could a stable system be achieved. However, this resulted in an insignificant effect on performance of the frequency response from force F to displacement z_1 and therefore these results are omitted.

Looking at the typical behaviour of RFC as shown in figure 6 it becomes clear that this instability might also be considered typical behaviour for this case. While simulated results show an increase in performance it must be noted that these simulations are based on a model of the system. Due to the lack of roll-off in the chosen controller, for the simulated performance to be achieved, the model of the system needs to be perfect. Figure 15 shows the open-loop frequency response of leafspring A with the optimally tuned RFC controller, up to the sampling frequency. This shows that instability is unavoidable. The dynamic behaviour of the measured frequency response from $V1a$ to $V1b$ differs from the simulated frequency response at high frequencies, presumably caused by non-collocated modes. Another contributing factor can be that in the experimental setup more delay is present than accounted for during the simulations.

Parameter variation

The parameter variations for PPF as listed in table 4 are divided in two categories where either the controller frequency or the combination of controller gain and damping is varied. As previously discussed these variations are such that the simulated results are outside of the optimal region ($< 2\%$) and are therefore expected to achieve less performance compared to the chosen optimally tuned parameter settings.

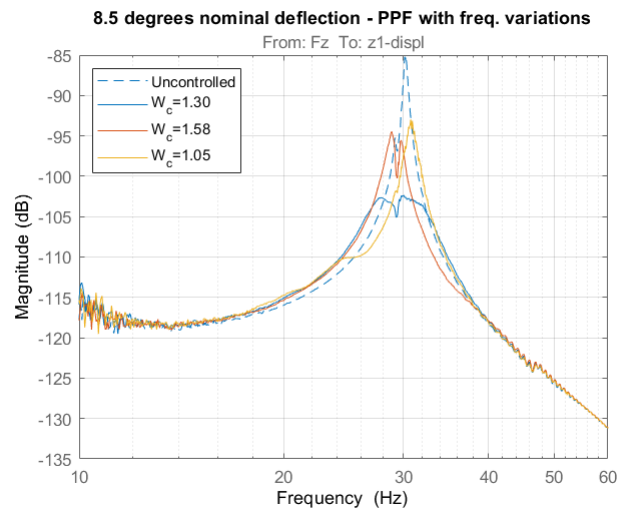


Figure 16. Frequency response from force F to displacement z_1 with PPF enabled with controller frequency variations

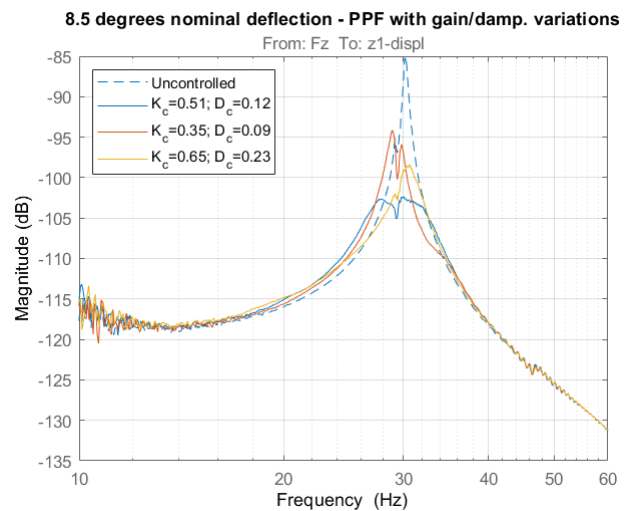


Figure 17. Frequency response from force F to displacement z_1 with PPF enabled with gain and damping factor variations

Figure 16 shows the effect of the variation in controller frequency on the frequency response from force F to displacement z_1 . Here, it can be seen that both an increase and a decrease in controller frequency leads to a decrease in applied damping on the resonance peak. There is also a slight shift of the resonance peak noticeable. Aside from this decrease in performance both variations appear to have no significant effect on the regions outside of this resonance peak.

Similarly to the previous, figure 17 shows the effect of the variation in the parameter combination of controller gain and controller damping. From this it can be seen that a combined increase and a combined decrease of the parameters also both lead to a decrease in applied damping on the resonance peak as well as a slight shift in resonance peak. These combined variations appear to have a more pronounced effect on the regions outside of the resonance peak.

Additional diagrams are in appendix D as well as the results for additional deflected states. These additional deflected states demonstrate similar behaviour.

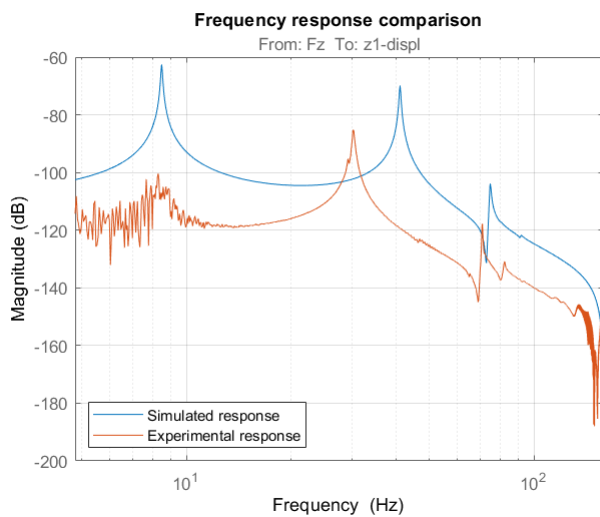


Figure 18. Comparison of simulated frequency response with experimental frequency response from force F to displacement z_1

Discussion and Recommendations

When comparing the experimental system identification results from appendix D with the simulated results from appendix B it becomes apparent that the system model contains slight inaccuracies since the frequency response data deviates from the simulated data. Figure 18 shows this comparison for the frequency response from force F to displacement z_1 . Some of these inaccuracies are likely caused by neglected dynamics. Additionally, the experimental frequency response shows a greater resonance peak in undeflected state than in the simulated data. This is to be expected as in undeflected state the model assumes the leafsprings to be perfectly aligned and as such the flexure hinge has great overall support stiffness. However, in practice, the leafsprings are most likely slightly misaligned and therefore the overall support stiffness is reduced.

As the model is the basis for which the controller parameters have been tuned, it should be noted that these inaccuracies potentially mean the tuned parameters are also inaccurate. However, the applied controllers are shown to be effective in damping the parasitic resonance from force F to displacement z_1 in both the simulated frequency response and the experimental frequency response, with similar performance. Therefore, it can be concluded that the model is an adequate representation of the system and the underlying assumptions are valid. This means any improvement of the system model can only lead to a further improvement in performance. Furthermore, figure 18 shows that, although the resonance peaks vary in frequency and height, both frequency responses show highly similar behaviour. As the controller parameters are derived in normalised form these variations in frequency and height of the parasitic resonance are therefore irrelevant. It should be noted that these qualitative differences are relevant when comparing PPF and RFC controllers. Due to the lack of high frequency roll-off of RFC these qualitative differences are the probable cause for the experienced instability.

The system identification of the experimental setup, as well as the simulated system identification both show that,

although the effect is noticeable, the studied mode is registered less by the top leafspring (B) than the bottom leafspring (A) as the bottom leafspring is more affected by gravity. However, since the piezoelectric patches are controlled identically in the current setup, this implies that the contribution of the top leafspring to the attenuation of the resonance peak is also less. This opens up possibilities for further research to determine whether different parameter settings for each of the leafsprings will improve overall performance with respect to disturbance rejection with possibly multi-mode suppression. This can be done by utilizing a differential voltage signal with a single controller or through the control scheme as depicted in figure 5 but with separate distinctive controllers. Alternatively, applying modal decomposition could be used to further investigate what modes have the greatest negative effect on overall performance and to better target those modes effectively.

In undeflected state the currently investigated controllers show only a limited performance increase compared to the deflected states but the resonance peak from force F to displacement z_1 was still present. This might indicate a greater contribution of the perpendicular leafsprings on performance than previously assumed which implicates these were wrongfully disregarded. This should be investigated further by placing additional piezoelectric elements on the perpendicular leafsprings. However, these leafsprings will likely experience mostly torsional strain when the system is in undeflected state. Even if the piezoelectric elements are selected accordingly, a significant increase in performance in undeflected state might prove difficult to achieve as torsion is challenging to couple with piezoelectric elements. The additional piezoelectric elements can be beneficial if the modal decomposition approach is to be used, as the amount of modes that can be decomposed is limited to the amount of sensors in the system.

Conclusion

A large stroke piezo damped flexure hinge has been extended with a second stage. This system has been developed for its ability to register parasitic modes of the end effector outside of the nominal movement plane. The displacement of the end effector in the direction perpendicular to the nominal movement has been selected as the mode of interest. For this mode an Active Vibration Damping control scheme has been presented. In this setup two controllers, Positive Position Feedback and Resonant Feedback Control, have been optimally tuned and compared for their performance in damping the selected parasitic mode. The tuning of the control parameters has been done through the proposed tuning method. The chosen performance criterion was the H2 norm of the transfer from force F to displacement z_1 . A grid search has been performed to determine optimal parameters for several deflected states and the means of these parameters have been selected. This resulted in an optimally tuned PPF controller and an optimally tuned RFC controller. Both of these controllers have been tested experimentally.

Experimental results show that the piezoelectric elements are able to register parasitic end-effector modes that are not visible in the nominal movement transfer. Although RFC showed similar simulated performance, its implementation

in the experimental setup led to instability and as such was an ineffective controller. PPF was proven to be an effective controller for damping the resonance of the mode of interest. Through parameter variation it has been shown that optimal controller parameters have been found for PPF. This has been proven for multiple states of deflection, although less so in undeflected state.

Through this work further insight was provided into how active vibration damping controller parameters can be tuned and this can ultimately lead to methods for optimal controller design in active vibration damping.

In this work the controllers have been limited to PPF and RFC and both of these controllers showed promising performance in simulations. Nevertheless only PPF proved to be an effective controller as RFC led to instability. Although the results from RFC show that high-frequency gain should be considered in a physical setup and the amount of feasible controllers might be limited by this, it is worth investigating how other control methods would perform in a similar setup.

Acknowledgements

The author wishes to thank; Prof. Dr. Ir. D.M. Brouwer PDEng, Dr. Ir. W. B. Hakvoort, Ir. B. Seinhorst, and everyone else who has contributed to this article.

References

- [1] S. Smith, *Flexures: Elements of Elastic Mechanisms*. 08 2000.
- [2] B. Seinhorst, M. Nijenhuis, and W. Hakvoort, "Design of a large deflection compliant mechanism with active material for vibration suppression," in *European Society for Precision Engineering and Nanotechnology, Conference Proceedings*, pp. 123–126, 2022.
- [3] M. Naves, R. Aarts, and D. Brouwer, "Large-stroke flexure hinges: Building-block-based spatial topology synthesis method for maximising flexure performance over their entire range of motion," *Mikroniek*, vol. 57, no. 3, pp. 5–9, 2017.
- [4] S. Peruvazhuthi and S. Gopalakrishnan, "Review on the use of piezoelectric materials for active vibration, noise, and flow control," *Smart Materials and Structures*, vol. 29, 02 2020.
- [5] A. Preumont and K. Seto, "Active control of structures," 2008.
- [6] B. Seinhorst, M. Nijenhuis, and W. Hakvoort, "Feasibility of active material vibration suppression in a large stroke flexure hinge," *IFAC-PapersOnLine*, vol. 55, no. 27, pp. 166–171, 2022.
- [7] Q. Mao and S. Pietrzko, *Positive Position Feedback (PPF) Control*, pp. 213–265. London: Springer London, 2013.
- [8] H. Syed, "Comparative study between positive position feedback and negative derivative feedback for vibration control of a flexible arm featuring piezoelectric actuator," *International Journal of Advanced Robotic Systems*, vol. 14, p. 172988141771880, 07 2017.
- [9] M. J. Balas, "Direct velocity feedback control of large space structures," *Journal of Guidance and Control*, vol. 2, no. 3, pp. 252–253, 1979.
- [10] B. Yang, "Vibration control of gyroscopic systems via direct velocity feedback," *Journal of Sound and Vibration*, vol. 175, no. 4, pp. 525–534, 1994.
- [11] A. Al-Mamun, E. Keikha, C. S. Bhatia, and T. H. Lee, "Integral resonant control for suppression of resonance in piezoelectric micro-actuator used in precision servomechanism," *Mechatronics*, vol. 23, no. 1, pp. 1–9, 2013.
- [12] S. S. Aphale, A. J. Fleming, and S. O. R. Moheimani, "Integral resonant control of collocated smart structures," *Smart Materials and Structures*, vol. 16, p. 439, feb 2007.
- [13] M. I. Friswell and D. J. Inman, "The relationship between positive position feedback and output feedback controllers," *Smart Materials and Structures*, vol. 8, p. 285, jun 1999.
- [14] V. den Ouden, "Design of a piezo damped flexure hinge demonstrator," Master's thesis, University of Twente, August 2022.
- [15] M. Naves, M. Nijenhuis, W. Hakvoort, and D. Brouwer, "Flexure-based 60 degrees stroke actuator suspension for a high torque iron core motor," *Precision engineering*, vol. 63, pp. 105–114, May 2020.
- [16] T. K. Caughey, "Dynamic response of structures constructed from smart materials," *Smart Materials and Structures*, vol. 4, p. A101, mar 1995.
- [17] J. Shan, H.-T. Liu, and D. Sun, "Slewing and vibration control of a single-link flexible manipulator by positive position feedback (ppf)," *Mechatronics*, vol. 15, no. 4, pp. 487–503, 2005.
- [18] MathWorks, *Matlab 2023a Control system toolbox documentation*. Available at: <https://nl.mathworks.com/help/control/ref/dynamicsystem.norm.html>.
- [19] J. van Dijk, "System and control design 2," 2013.
- [20] Tecnotion, *UM Series Ironless datasheet*. Available at: <https://www.tecnotion.com/products/ironless-motors-um-series/>.
- [21] Maxon, *ESCON 50/5 Servocontroller datasheet*. Available at: <https://www.maxongroup.com/maxon/view/product/control/4-Q-Servokontroller/409510>.
- [22] RLS, *LM10 Encoder datasheet*. Available at: <https://www.rls.si/eng/lm10-linear-and-rotary-magnetic-encoder-system>.
- [23] Endevco, *Piezoelectric accelerometer datasheet*. Available at: <https://buy.endevco.com/accelerometer/7703a-accelerometer-2>.
- [24] Smart Material, *Macro Fiber Composite Overview*. Available at: <https://www.smart-material.com/MFC-product-mainV2.html>.
- [25] Hasberg Schneider GmbH, *Material Technical Information*. Available at: <https://www.hasberg-schneider.de/en/services/technical-information/>.
- [26] Akribis Systems, *AVM Series Technical Data*. Available at: <https://akribis-sys.com/products/voice-coil-motors/avm-series>.
- [27] RLS, *LM13 Encoder datasheet*. Available at: <https://www.rls.si/eng/lm13-magnetic-linear-and-rotary-encoder-system>.
- [28] J. van Dijk and R. Aarts, "Analytical one parameter method for pid motion controller settings," in *Proceedings of the IFAC Conference on Advances in PID Control, WeC2.4*, pp. 1–6, University of Brescia, 2012.

Shaker element design

The second motion stage of the setup is to be used as a shaker element to accurately determine the transfer of the tip of the first motion stage from force to displacement. In previous research this has been done through the use of a mode impact hammer, though it was decided to integrate a shaker in the setup to ease experimental verification.

A.1 Requirements

The design requirements of the shaker element are the following:

- The shaker element should constrain all degrees of freedom except for translation in z-direction.
- The parasitic resonance frequency on which damping is to be applied shifts with nominal deflection. To prevent interference on the parasitic resonance the eigenfrequencies of the shaker element should be outside of this region. Therefore, the first eigenfrequency should be below 10 Hz and the second eigenfrequency should be above 100 Hz.
- The previously used end-effector was a brass mass of around 0.75kg. The new design should be of similar mass to retain the applicability of previously drawn conclusions.

A.2 Constraints

In addition to the previous requirements there are several constraints. These mainly revolve around equipment availability. Although these are not

- The available encoder is a RLS LM13. The LM13 is a contactless high-speed linear magnetic system designed for linear or rotary motion sensing. It has a resolution of 1 μ m. [27]
- The available actuator is an Akribis AVM30-15. The AVM30-15 is a permanent-magnet direct drive voice coil motor. It has a stroke length of 15 mm and can apply a continuous force of 4.63N. [26]
- The available flexure material is RVS 14.310. It is a chromium nickel stainless steel alloy with a Young's modulus of 190 GPa and a shear modulus of 73 GPa. [25]

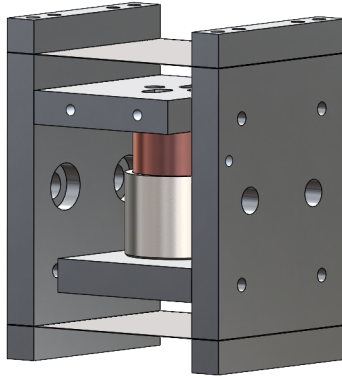


Figure A.1: Shaker element model

Table A.1: Leafspring dimensions

Parameter	Value
Length	79 mm
Width	60 mm
Thickness	0.2 mm

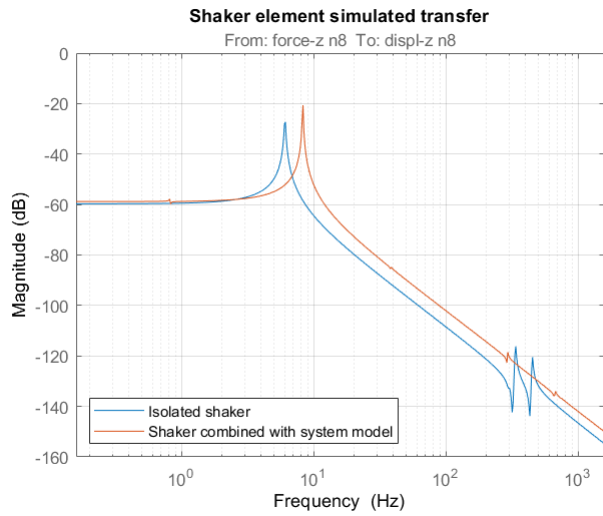


Figure A.2: Shaker bode

Table A.2: Modal frequencies

Mode	Frequency (Hz)
1	6.049
2	205.1
3	264.9
4	298.5

A.3 Dimensions

The previous has led to the design of a simple two leaf parallel straight guide shown in figure A.1. The dimensions of the two leafsprings are listed in table A.1. The design has been analysed through the use of SPACAR software. The projected movement mass sag due to gravity is around 6.7 mm which is within the maximum stroke of the VCM. Furthermore, the total mass of the shaker element is around 0.6kg which is expected to be close enough to the previously used mass for the model to be accurate.

The modal frequency results from SPACAR are listed in table A.2. The first eigenfrequency of the shaker element is around 6 Hz which is well below the lower boundary of 10 Hz. The second eigenfrequency is around 205 Hz which is well above the upper boundary of 100 Hz. After incorporation of the shaker element in the complete system model these values shift slightly as the base of the shaker is no longer rigidly connected to the fixed world but instead it is fixed to the first stage. The resulting first eigenfrequency of the shaker is around 8.5 Hz which is also well below the lower boundary. Figure A.2 shows the bode magnitude diagram of force F to displacement z_2 for both the isolated shaker element and the shaker element incorporated in the system model where the shift in the first eigenfrequency is clearly visible. It should be noted that the second eigenfrequency of the shaker element, at around 200 Hz, is not visible in figure A.2 as it is an internal leafspring mode, i.e. has no effect on z-displacement of the movement mass.

Simulation results

B.1 System Model Frequency Response

Figure B.1 shows the full 5x4 system - with inputs $M, F, V1a, V2a$ and outputs $\theta, z_1, z_2, V1b, V2b$ - simulated frequency response for four states of deflection; undeflected, 2.8 degrees nominal deflection, 5.7 degrees nominal deflection, and 8.5 degrees nominal deflection. For these results a modal damping of 0.5% is assumed.

B.2 Parameter Sweeps

The parameter sweeps over the controller gain, controller damping, and controller frequency have been performed for both controller options, PPF and RFC, for three deflected states; 2.8 degrees nominal deflection, 5.7 degrees nominal deflection, and 8.5 degrees nominal deflection. The results of these parameter sweeps are included in this appendix.

Positive Position Feedback

Figure B.2 shows the simulation results with PPF enabled at 2.8 degrees nominal deflection. Here figure B.2a shows the sensitivity surface as seen from the frequency-damping plane, figure B.2b shows the sensitivity surface as seen from the damping-gain plane, and figure B.2d shows the sensitivity surface as seen from the frequency-gain plane. Figure B.2c shows an isometric view of the sensitivity surface. This display style is used throughout this appendix.

Figure B.3 shows the simulation results with PPF enabled at 5.7 degrees nominal deflection and figure B.4 shows the simulation results with PPF enabled at 8.5 degrees deflection.

Resonant Feedback Control

Similar to PPF, figures B.5, B.6, and B.7 show the simulation results with RFC enabled at 2.8 degrees, 5.7 degrees, and 8.5 degrees nominal deflection, respectively.

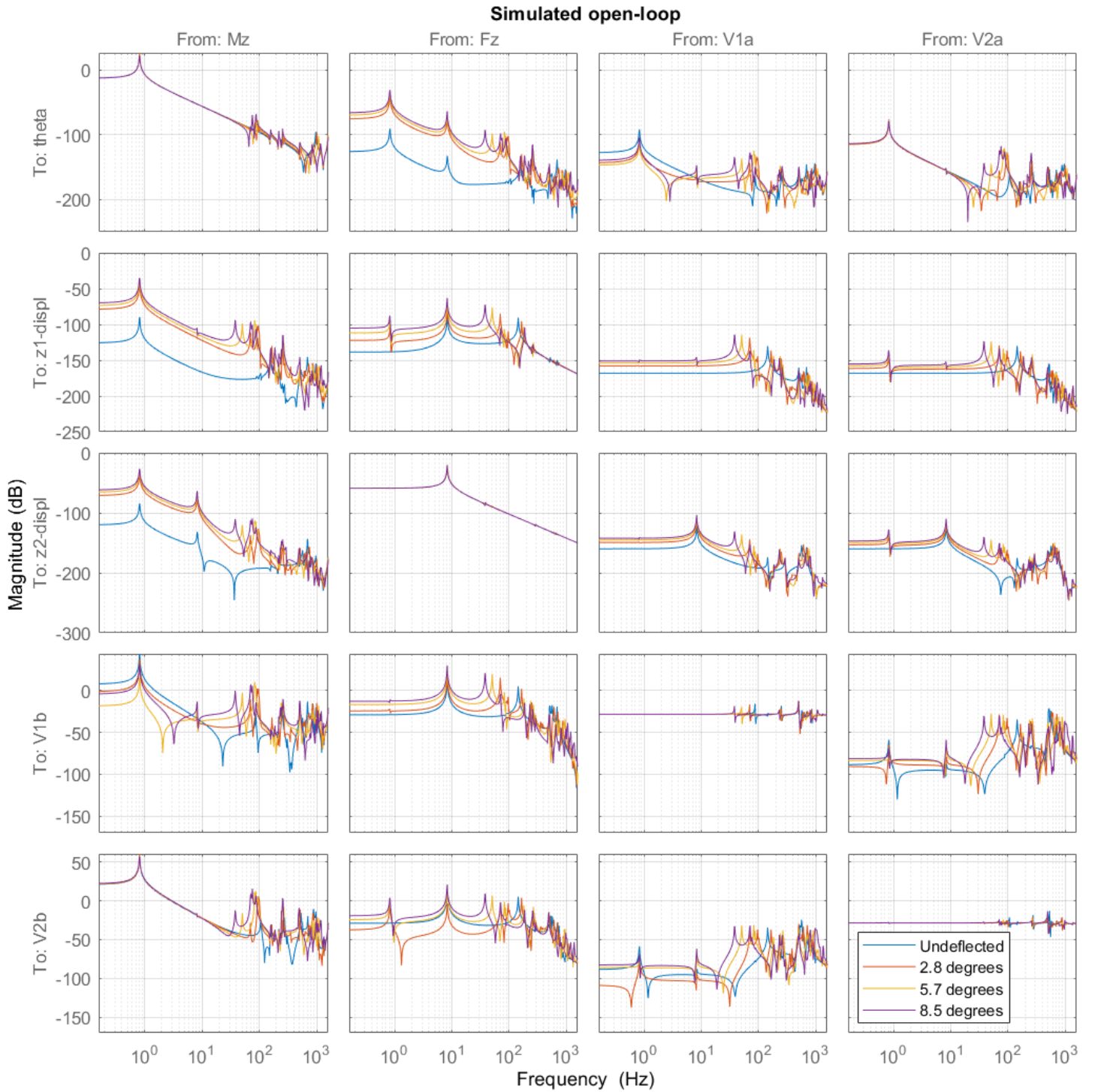


Figure B.1: Simulated frequency response of the open-loop system

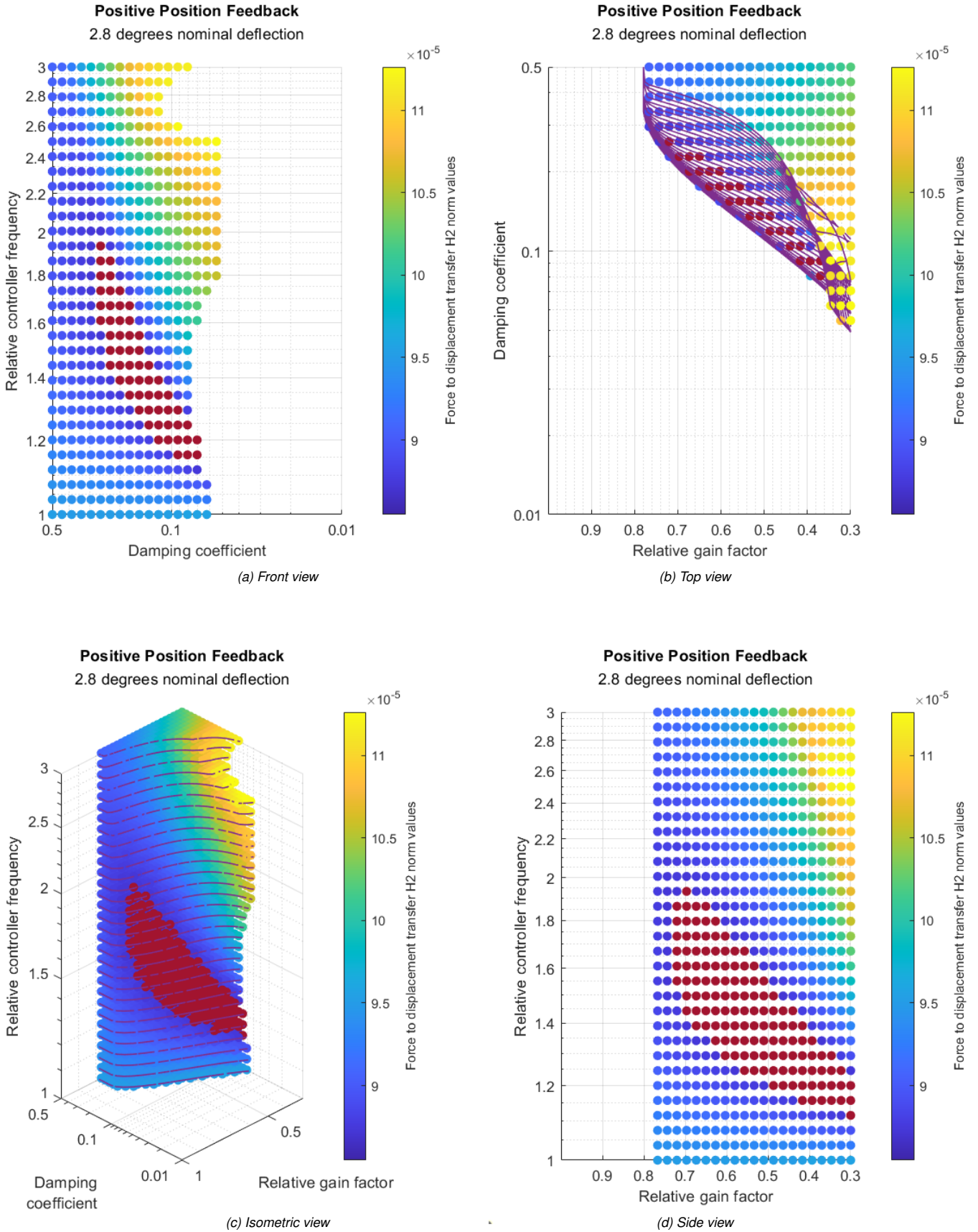


Figure B.2: 2D projection for H2 norm calculations for PPF under 2.8 degrees of deflection

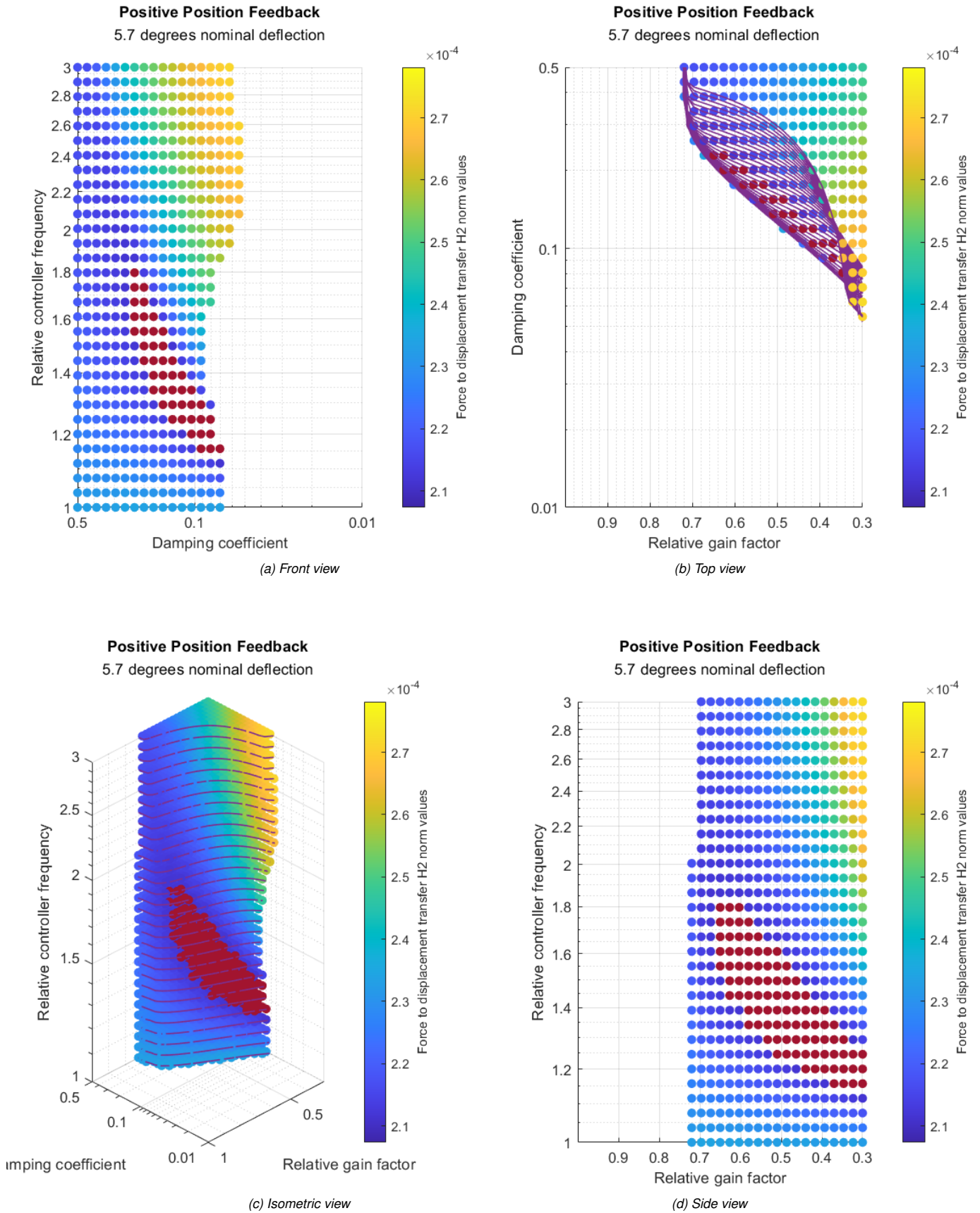


Figure B.3: 2D pojection for H2 norm calculations for PPF under 5.7 degrees of deflection

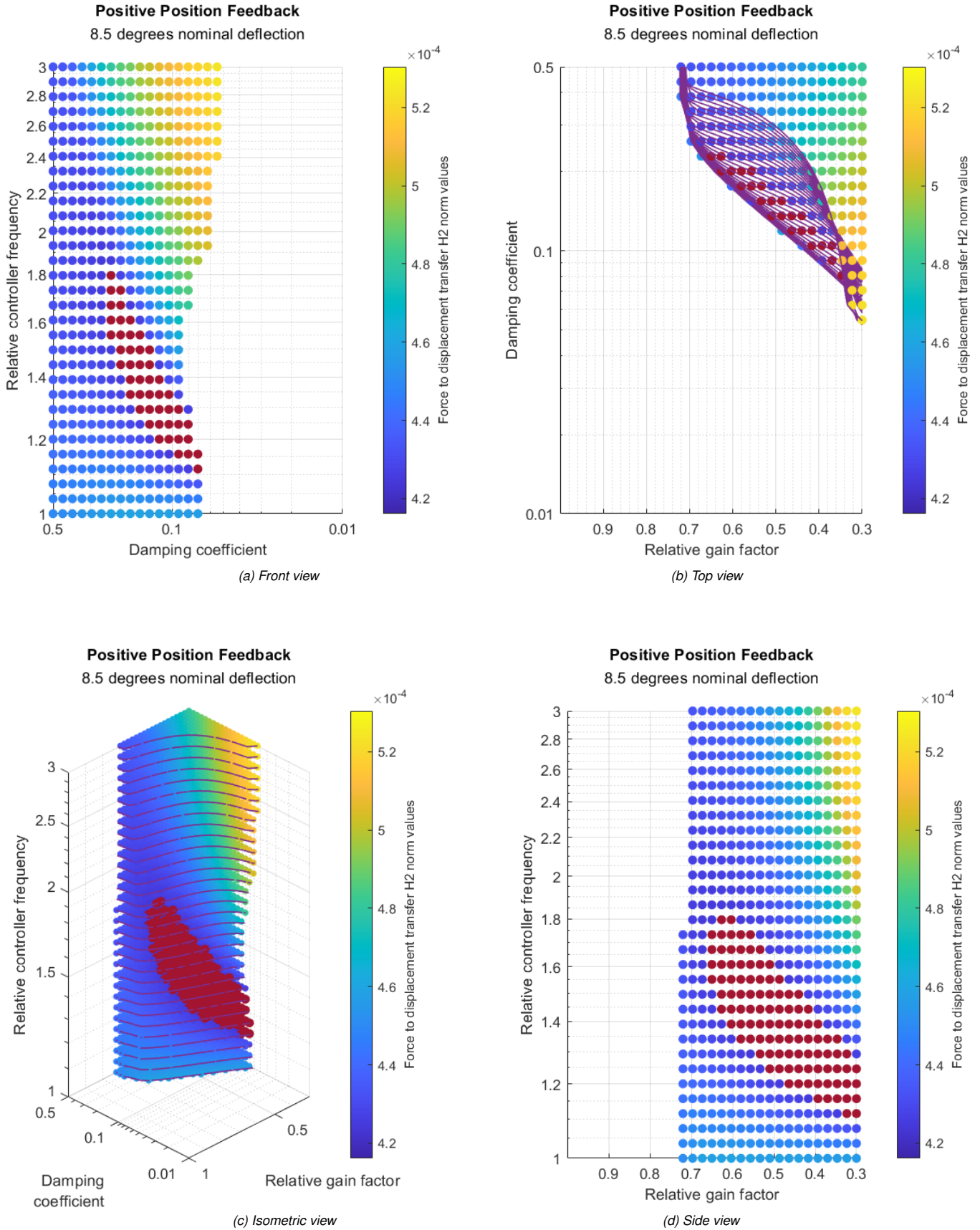


Figure B.4: 2D projection for H2 norm calculations for PPF under 8.5 degrees of deflection

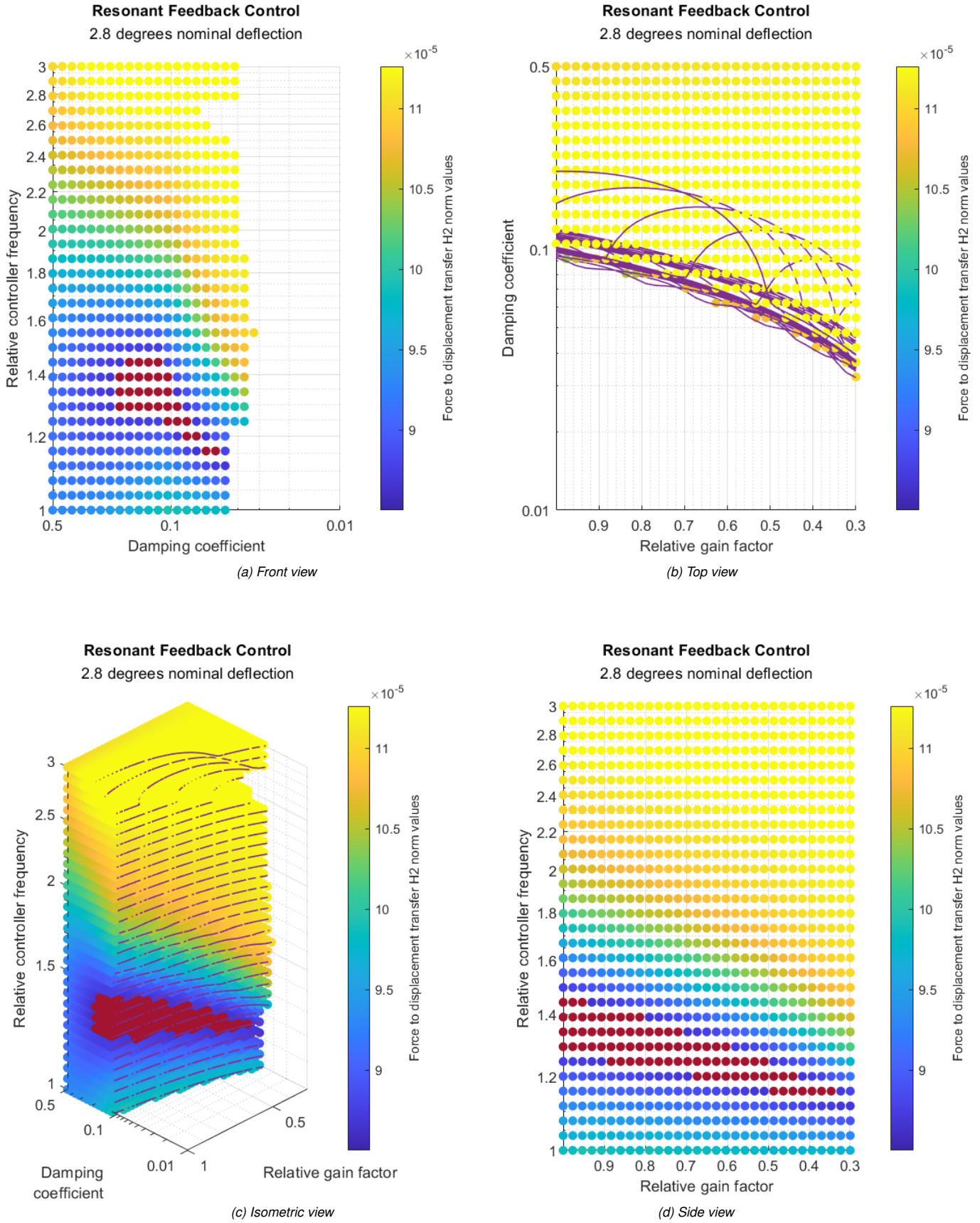


Figure B.5: 2D projection for H2 norm calculations for RFC under 2.8 degrees of deflection

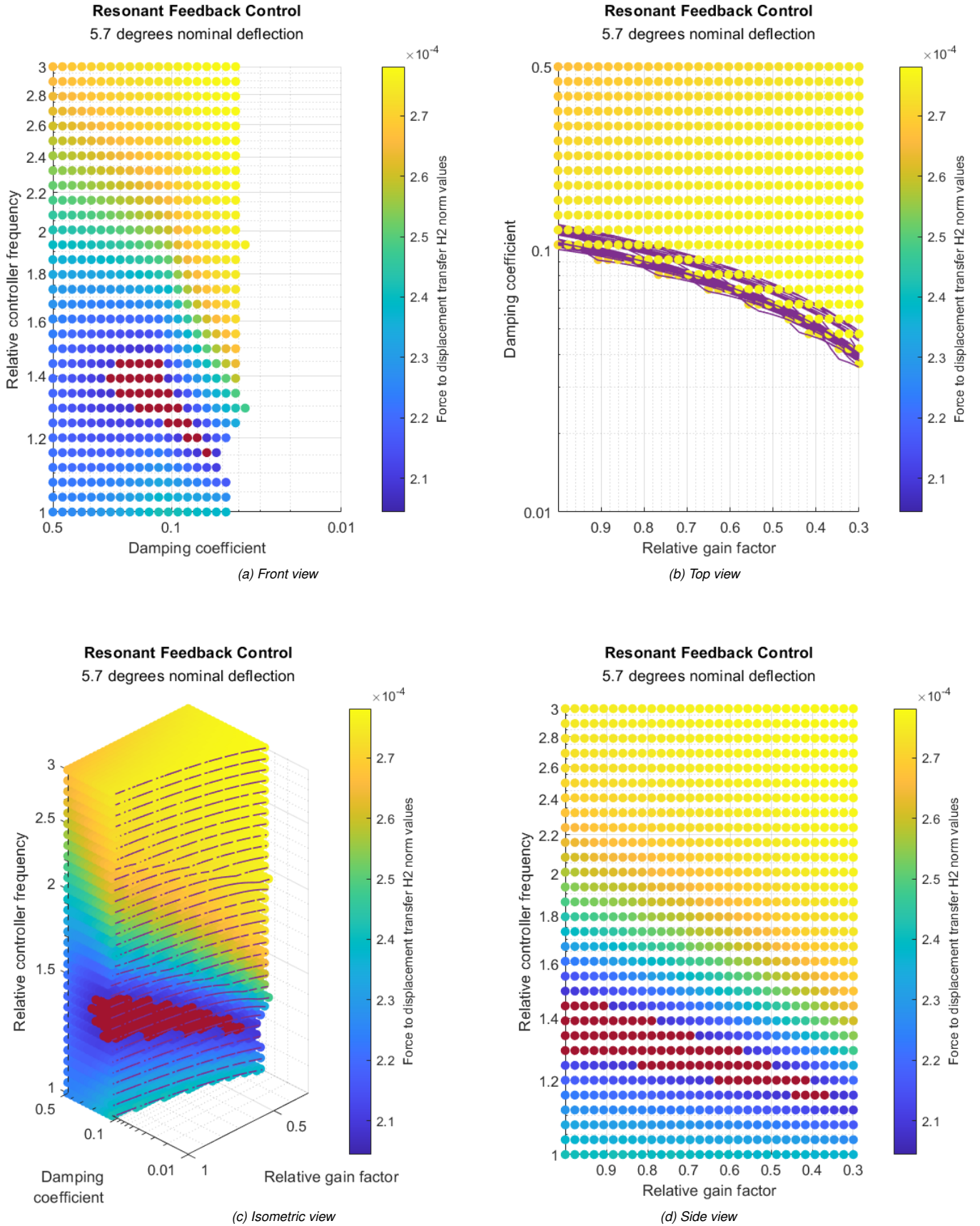


Figure B.6: 2D projection for H2 norm calculations for RFC under 5.7 degrees of deflection

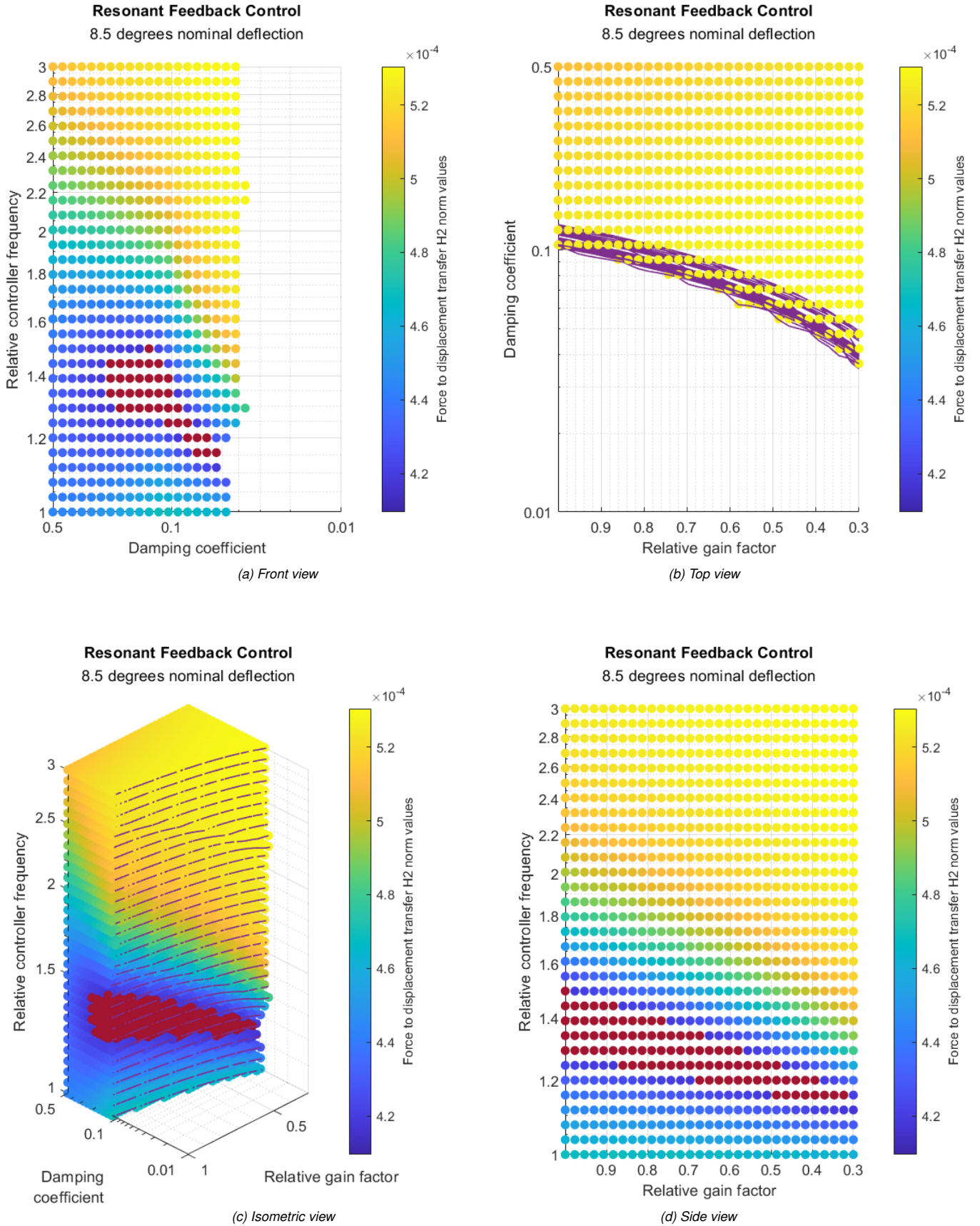


Figure B.7: 2D projection for H2 norm calculations for RFC under 8.5 degrees of deflection

Experimental setup

In this appendix several pictures are included of the experimental setup where figure C.1 shows an overview of the setup, figure C.2 shows the top view of the setup in undeflected state, and figure C.3 shows the top view of the setup in deflected state at 8.5 degrees nominal deflection.

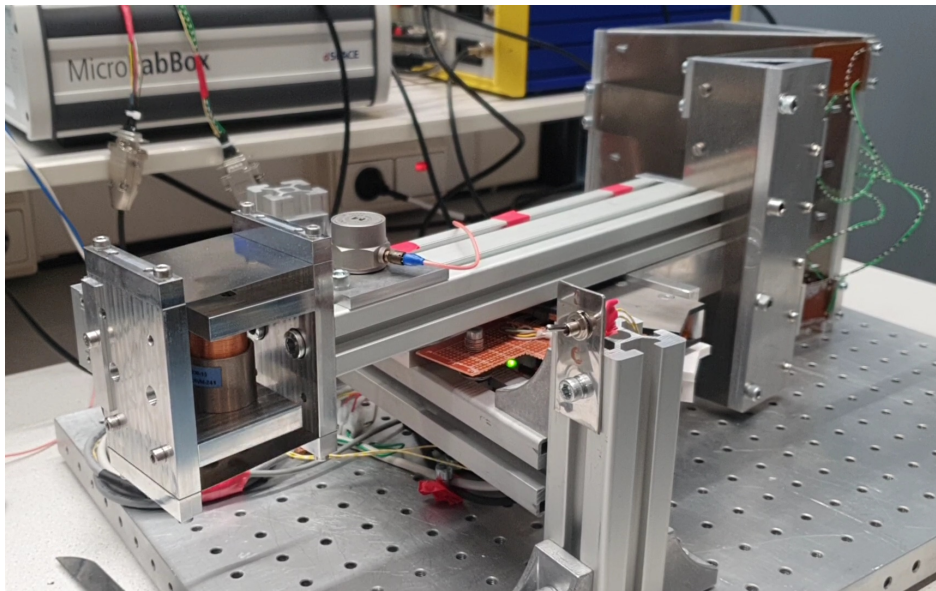


Figure C.1: Picture of experimental setup overview

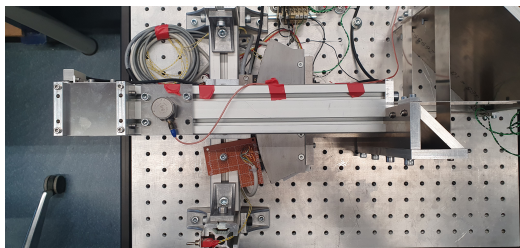


Figure C.2: Undeflected state of experimental setup

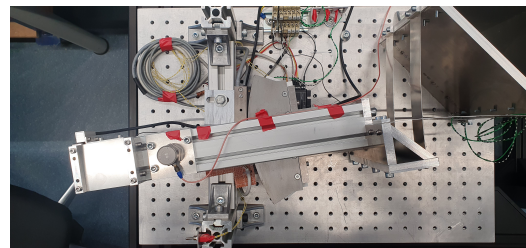


Figure C.3: Deflected at 8.5 degrees nominal deflection of experimental setup

Experimental results

D.1 Frequency Response Estimate

The dynamics of the system identified through the use of a chirp signal. This method is used for both with and without active damping enabled. Normally these results can be classified as open-loop behaviour and closed-loop behaviour. However, as the dynamics of the flexure hinge change drastically with a change in nominal deflection, it is crucial to retain certain positions during testing. Therefore, in this case the system identification results are classified as “partially open-loop” and “closed loop”. Figure D.1 illustrates this difference. Here, $P(s)$ refers to the open-loop transfer of the system and $\tilde{P}(s)$, the area shaded in grey, refers to the partially open-loop transfer. The frequency response data of this partially open loop system is shown in figure D.2.

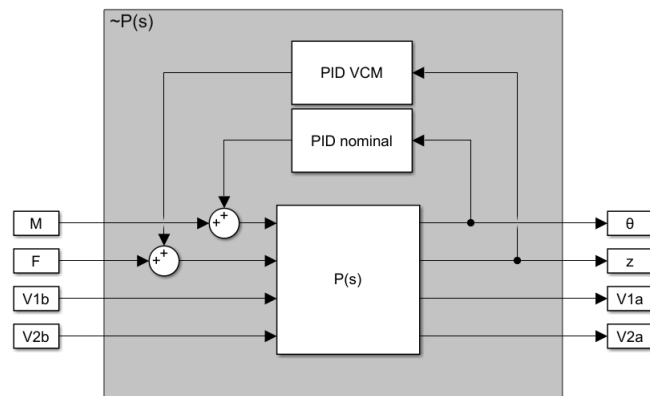


Figure D.1: Schematic for partially open-loop system $\tilde{P}(s)$ used for system identification

D.2 Optimally tuned PPF controller

Figure D.3 shows the frequency response data of the closed loop system, with the optimally tuned PPF controller enabled.

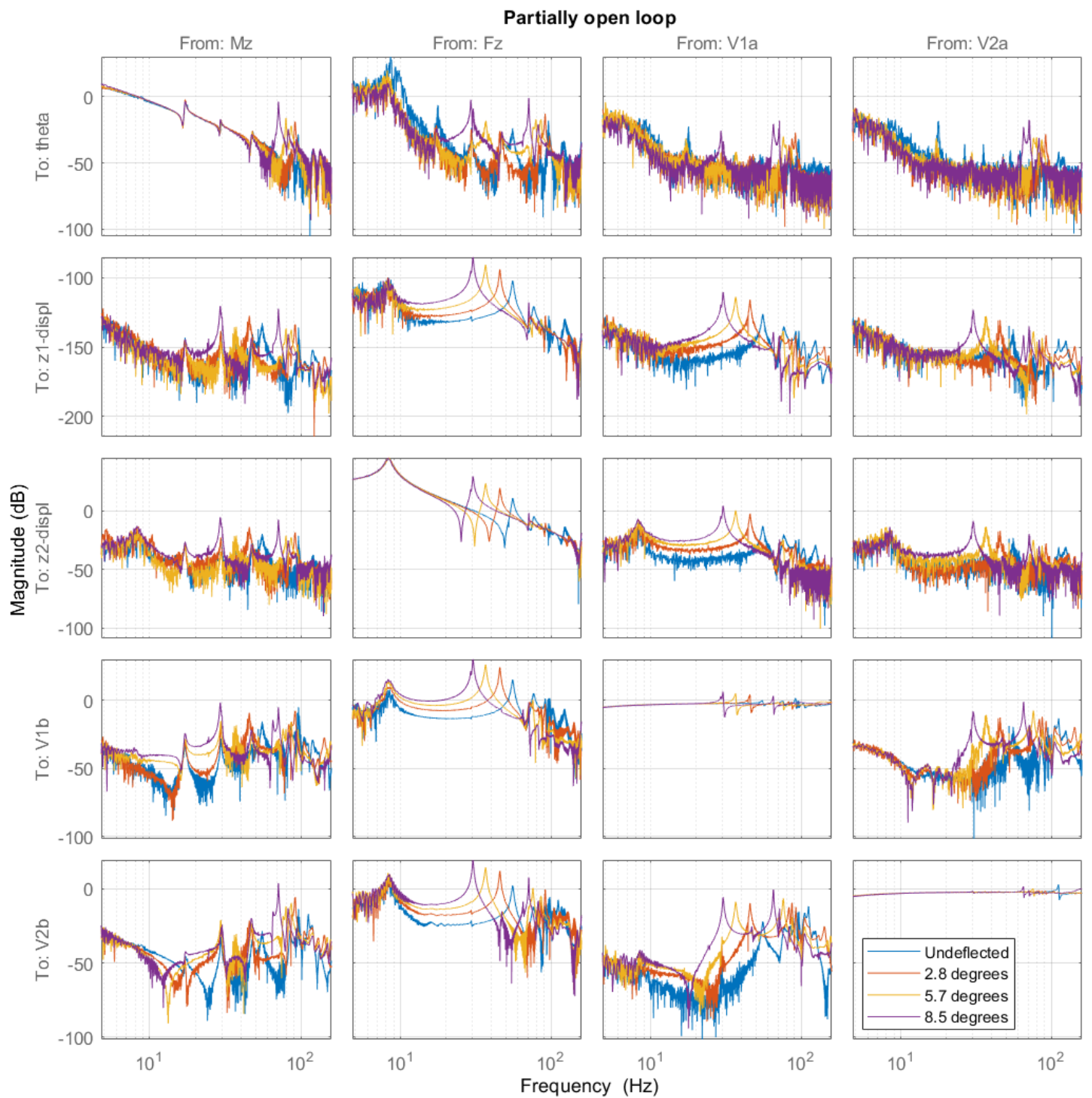


Figure D.2: Frequency response estimate of the partially open-loop system $\hat{P}(s)$ as depicted in figure D.2

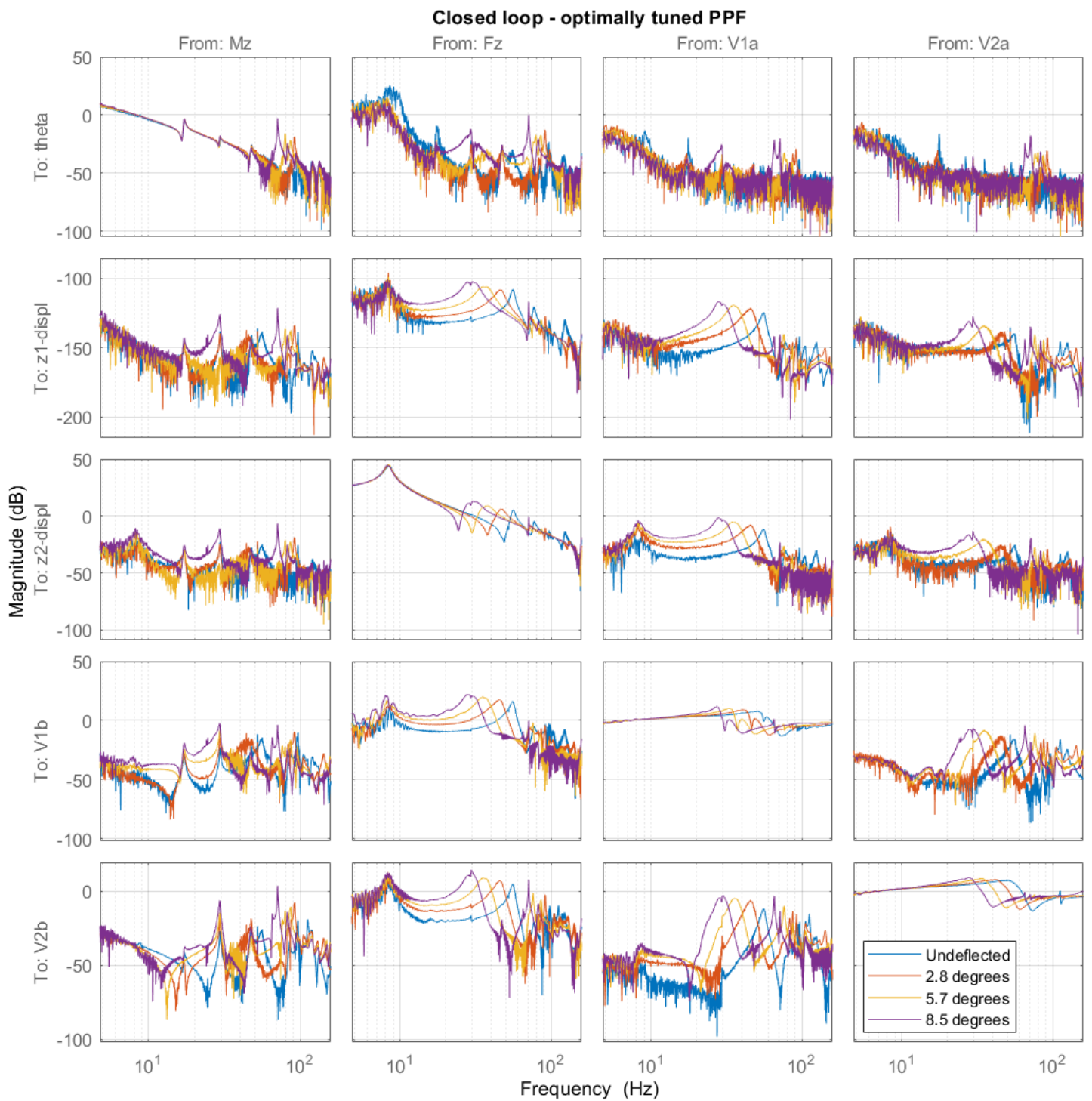


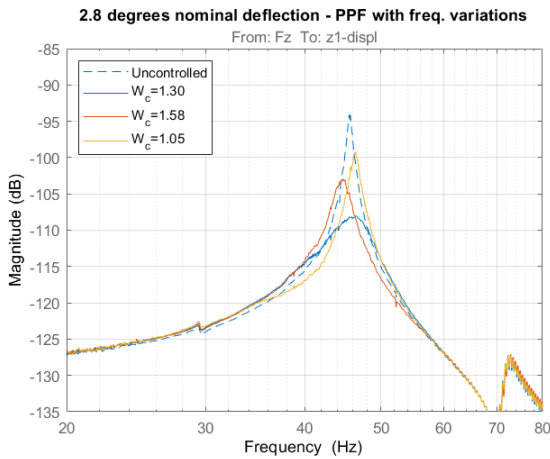
Figure D.3: Frequency response estimate of the closed-loop system with the optimally tuned PPF controller enabled

D.3 Frequency variation

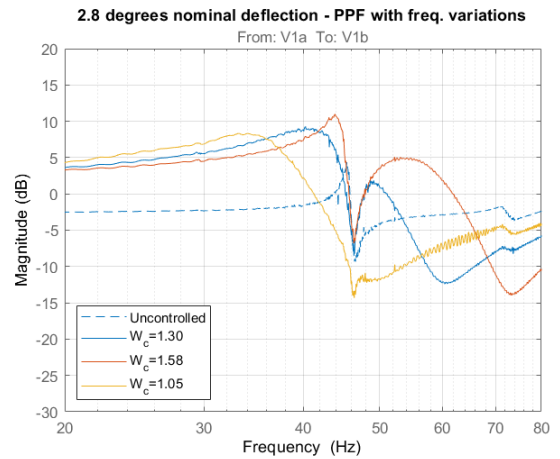
The frequency variations have been performed for three deflected states; 2.8 degrees nominal deflection, 5.7 degrees nominal deflection, and 8.5 degrees nominal deflection. Figure D.4 shows the results of these variations for the 2.8 degrees nominal deflection case. Here, figure D.4a shows the frequency response of force F_z to displacement z_1 around the parasitic resonance frequency. Figure D.4b shows the accompanying frequency response of voltage $V1a$ to voltage $V1b$. Similarly, figures D.5 and D.6 show the frequency variation results for the 5.7 degrees nominal deflection and 8.5 degrees nominal deflection cases, respectively.

D.4 Gain/damping variation

The gain/damping variations have been performed for three deflected states; 2.8 degrees nominal deflection, 5.7 degrees nominal deflection, and 8.5 degrees nominal deflection. Figure D.7 shows the results of these variations for the 2.8 degrees nominal deflection case. Here, figure D.7a shows the frequency response of force F_z to displacement z_1 around the parasitic resonance frequency. Figure D.7b shows the accompanying frequency response of voltage $V1a$ to voltage $V1b$. Similarly, figures D.8 and D.9 show the frequency variation results for the 5.7 degrees nominal deflection and 8.5 degrees nominal deflection cases, respectively.

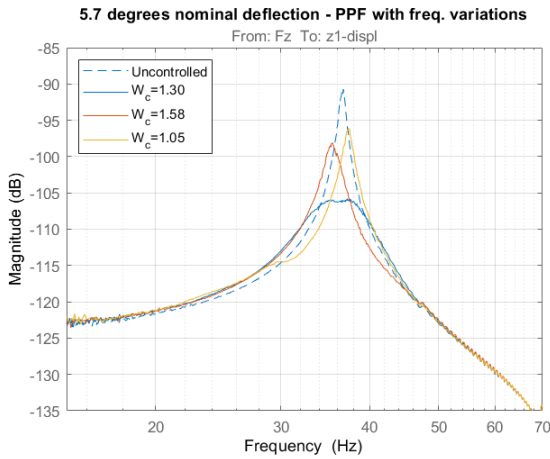


(a) Frequency response data from force F_z to displacement z_1

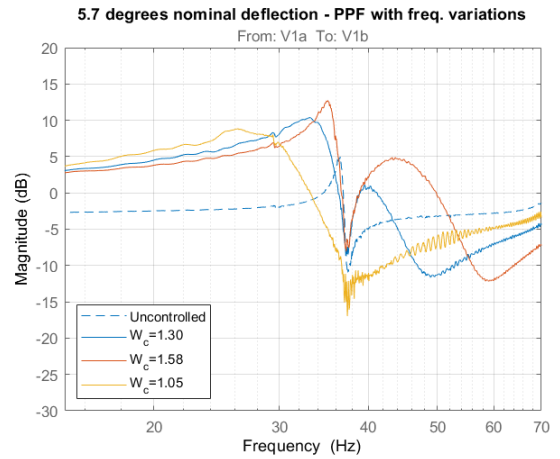


(b) Frequency response data from voltage V_{1a} to voltage V_{1b}

Figure D.4: Optimally tuned PPF and frequency variations for 2.8 degrees nominal deflection

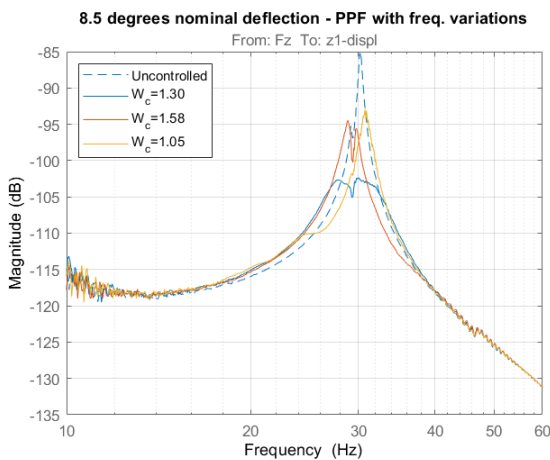


(a) Frequency response data from force F_z to displacement z_1

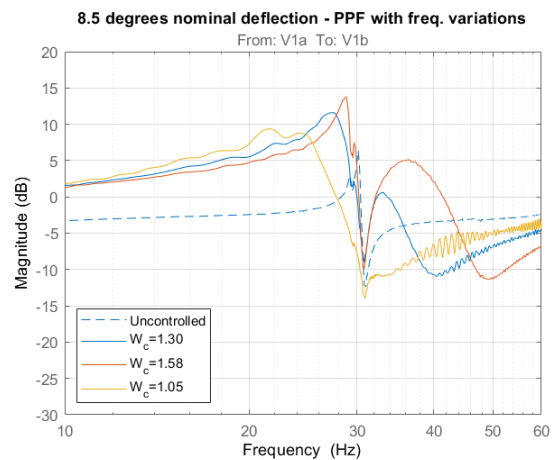


(b) Frequency response data from voltage V_{1a} to voltage V_{1b}

Figure D.5: Optimally tuned PPF and frequency variations for 5.7 degrees nominal deflection

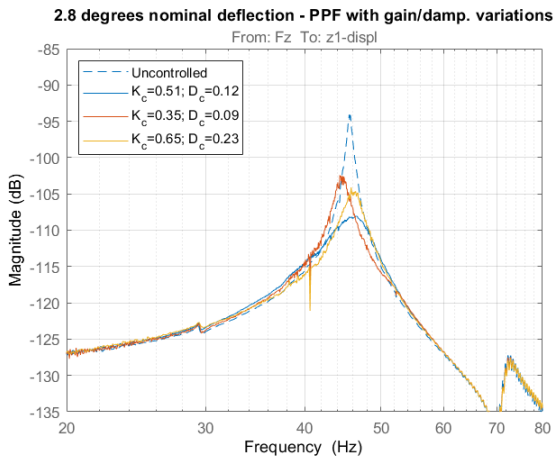


(a) Frequency response data from force F_z to displacement z_1

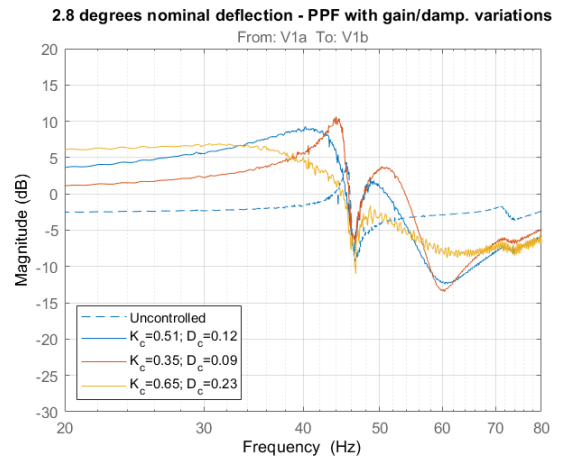


(b) Frequency response data from voltage V_{1a} to voltage V_{1b}

Figure D.6: Optimally tuned PPF and frequency variations for 8.5 degrees nominal deflection

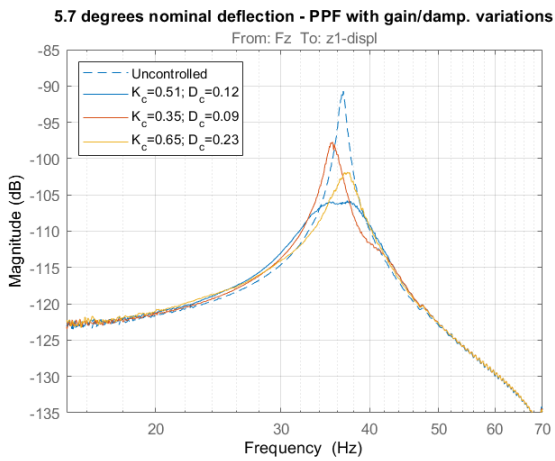


(a) Frequency response data from force F_z to displacement z_1

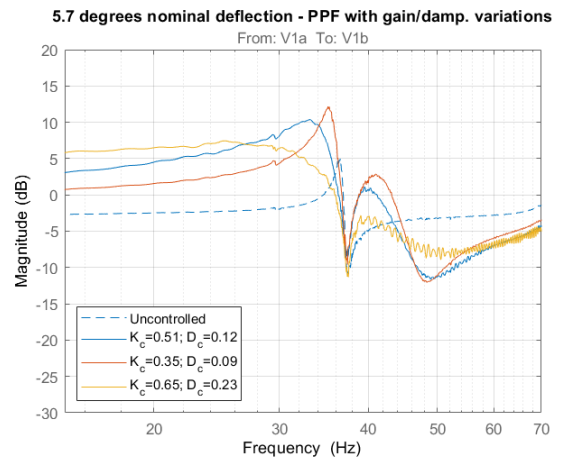


(b) Frequency response data from voltage V_{1a} to voltage V_{1b}

Figure D.7: Optimally tuned PPF and gain/damping variations for 2.8 degrees nominal deflection

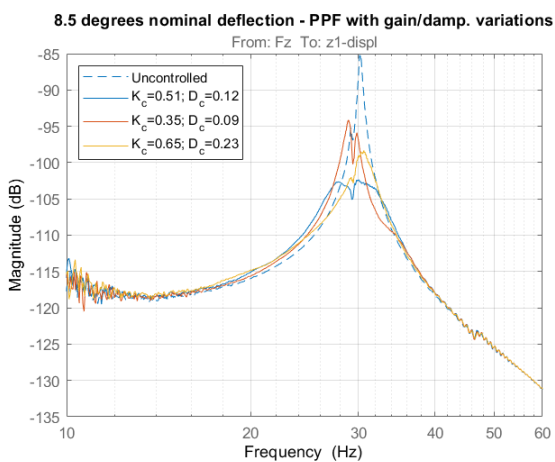


(a) Frequency response data from force F_z to displacement z_1

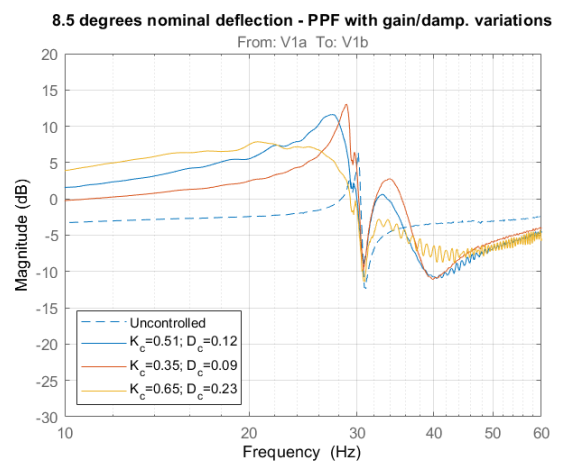


(b) Frequency response data from voltage V_{1a} to voltage V_{1b}

Figure D.8: Optimally tuned PPF and gain/damping variations for 5.7 degrees nominal deflection



(a) Frequency response data from force F_z to displacement z_1



(b) Frequency response data from voltage V_{1a} to voltage V_{1b}

Figure D.9: Optimally tuned PPF and gain/damping variations for 8.5 degrees nominal deflection